

Review

# Recent Advances in Mussel-Inspired Synthetic Polymers as Marine Antifouling Coatings

Ioannis Manolakis <sup>1,2,\*</sup>  and Usaid Azhar <sup>1,2</sup>

<sup>1</sup> Precision Engineering, Materials & Manufacturing (PEM) Research Centre, Institute of Technology Sligo, Ash Lane, F91 YW50 Sligo, Ireland; [usaid.azhara@mail.itsligo.ie](mailto:usaid.azhara@mail.itsligo.ie)

<sup>2</sup> Department of Life Sciences, Faculty of Science, Institute of Technology Sligo, Ash Lane, F91 YW50 Sligo, Ireland

\* Correspondence: [manolakis.ioannis@itsligo.ie](mailto:manolakis.ioannis@itsligo.ie)

Received: 15 June 2020; Accepted: 2 July 2020; Published: 7 July 2020



**Abstract:** Synthetic oligomers and polymers inspired by the multifunctional tethering system (byssus) of the common mussel (genus *Mytilus*) have emerged since the 1980s as a very active research domain within the wider bioinspired and biomimetic materials arena. The unique combination of strong underwater adhesion, robust mechanical properties and self-healing capacity has been linked to a large extent to the presence of the unusual  $\alpha$ -amino acid derivative L-DOPA (L-3,4-dihydroxyphenylalanine) as a building block of the mussel byssus proteins. This paper provides a short overview of marine biofouling, discussing the different marine biofouling species and natural defenses against these, as well as biomimicry as a concept investigated in the marine antifouling context. A detailed discussion of the literature on the *Mytilus* mussel family follows, covering elements of their biology, biochemistry and the specific measures adopted by these mussels to utilise their L-DOPA-rich protein sequences (and specifically the *ortho*-bisphenol (catechol) moiety) in their benefit. A comprehensive account is then given of the key catechol chemistries (covalent and non-covalent/intermolecular) relevant to adhesion, cohesion and self-healing, as well as of some of the most characteristic mussel protein synthetic mimics reported over the past 30 years and the related polymer functionalisation strategies with L-DOPA/catechol. Lastly, we review some of the most recent advances in such mussel-inspired synthetic oligomers and polymers, claimed as specifically aimed or intended for use in marine antifouling coatings and/or tested against marine biofouling species.

**Keywords:** mussel adhesive proteins; L-DOPA; catechol; bio-inspired synthetic polymers; adhesion; marine antifouling

## 1. Introduction

Marine biofouling refers to the undesired attachment of various marine organisms on artificial structures present in seawater or freshwater environment. The diversity of marine ecosystems brings a plethora of organisms that can potentially adhere on essentially any material surface (metal, ceramic, plastic). Marine fouling species vary from microfoulers (e.g., bacteria, spores, diatoms, larvae) to macrofoulers (e.g., algae, seaweed, barnacles, mussels) with dimensions increasing from microns to centimeters, respectively [1].

Boat and ship hulls, pier columns, offshore wind turbines/oil platforms, heat exchangers and aquaculture infrastructure are some of the marine structures on which biofouling would occur, and which would in turn suffer significant deterioration in their operation and performance. For example, fouled hulls of marine vessels would lead to increased hydrodynamic drag forces and thus increased fuel consumption and elevated greenhouse gas emissions. The presence of

biofouling on marine structures requires cleaning and preventive maintenance, with the associated costs and operational downtime.

The economic and environmental impact of marine biofouling cannot be underestimated. The majority of global trade is carried out by sea, and the overall commercial marine coatings market size is forecast to exceed 15 billion USD by 2024 [2]. Moreover, the annual cost associated with biofouling for a class of middle-sized destroyer vessels of the US Navy was estimated at 56 million USD in 2011 [3]. Apart from increased fuel consumption and carbon emissions, a vessel with a fouled hull on a long-haul journey may transfer marine species in ecosystems where these would not normally be found. Invasive species can pose a significant threat to ecosystems by displacing the native populations. Furthermore, the direct costs related with addressing biofouling in the marine aquaculture sector have been estimated to 5–10% of the production costs, and with the indirect impact remaining to a large extent unknown [4].

The documented use of antifouling coatings on marine vessel hulls dates to the 17th century [5]. As a result, marine antifouling coatings (or antifouling paints as commercially known, encompassing a variety of products such as primers, topcoats, sealants, varnishes) are a mature and established technology, with the antifouling action historically achieved with the use of metal-based biocide compounds (mainly with copper and tin) as part of the coating formulation. However, environmental concerns and stricter regulatory guidelines have posed many challenges to the traditional and otherwise successful marine antifouling products. The International Maritime Organisation (IMO) issued a global prohibition of application (2003) and any further use (2008) of antifouling coatings using organotin-based biocidal compounds [6,7], due to their detrimental effects on non-targeted species of marine ecosystems and on aquaculture industries.

Despite the subsequent dominance of copper-based biocidal products and the emergence of additional biocide compound options (e.g., booster biocides, comprising nitrogen and sulfur heterocyclics and zinc organometallic compounds used in conjunction with copper to enhance its efficiency and broaden its spectrum), the pressure on antifouling paint manufacturers with respect to the environmental impact of biocides has been continuously increasing. For instance, the European Biocidal Products Regulation (BPR, EU Regulation 528/2012 [8]) published in 2012 has resulted in additional restrictions in antifouling paint composition (e.g., the proposed ban of the booster biocidal compound cybutryne, a diamino-1,3,5-triazine [9]). Inevitably, concerns on the use of copper and other biocidal compounds will continue to grow, as will the regulatory scrutiny on such long-established and otherwise successful products.

At the same time, the pressure on conventional marine antifouling paints could incentivise innovation in non-biocidal antifouling coatings. These are antifouling coating systems that would not depend on a biocidal compound to prevent biofouling. Some of the main categories in biocidal-free coatings are [1,5,10]:

- Anti-adhesive/foul-release coatings: such coating systems are usually based on hydrophobic/low surface energy polymers (e.g., silicones, fluoropolymers) which hinder the attachment or weaken the adhesive bond strength of biofouling species with their surface. However, it is the aforementioned hydrophobic and low surface energy nature of the polymer binder in these coatings that also makes the adhesion of the coating to the substrate (to be protected) problematic.
- Coatings based on poly(ethylene glycol)s, PEGs: PEGylation is a universal surface modification strategy across a number of industrial sectors, exploiting the hydrophilic nature of these polymers in order to prevent protein adsorption and subsequent fouling.
- Self-polishing non-biocidal coatings: the top layer of the paint on which biofouling occurs is hydrolysable and hence sacrificial, and is continuously depleted (along with the fouling organisms). In contrast to the self-polishing copolymer (SPC) biocidal coatings which rely on the release and action of a biocidal compound as the polymer binder hydrolyses and erodes from the coating, the self-polishing non-biocidal counterparts rely exclusively on the sacrificial surface layer to remove fouling.

Despite the intense research interest in these non-biocidal-based solutions, matching the market volume demand and product performance, durability and customer acceptance of existing biocide-containing commercial products and ultimately claiming a market share remain a major challenge.

Amongst the various efforts reported towards environmentally friendly biocidal-free coatings, a biomimetic approach has been widely proposed: seek inspiration from nature, and in fact, it has been the actual biofouling species and/or the natural defenses against these (e.g., surface chemistry, surface topography) which provide valuable information on how to design efficient antifouling material solutions—from and for the marine domain, and not only [1,5,7,11–14].

In this research field of bioinspired and biomimetic materials for antifouling applications, mussel-inspired polymers and coatings have had a prominent position since the pioneering work of Herbert Waite in the early 1980s [15]. The remarkable ability of mussels to attach onto virtually any surface underwater has prompted extensive scientific interest on developing synthetic polymers and oligomers that mimic the structure of the mussel adhesive proteins (MAPs) which are key to this process. The central feature of mussel-inspired adhesion is that it is mediated via a number of 3,4-dihydroxyphenyl (catechol) moieties present in the structure, and a range of related non-covalent interactions.

A wide variety of mussel-inspired synthetic polymers and their functional coatings have been since reported, including *marine antifouling coatings*: using a polymer with mussel-inspired adhesion as a coating against fouling species present in the marine environment. Recent advances in this specific domain would be highlighted in this review.

## 2. Marine Biofouling: Mechanisms, Natural Defenses and Biomimicry

It is universally accepted [1,5,7,10,16,17] that the fouling process starts in essence immediately after a surface has been immersed in either seawater or freshwater. The process begins with the adsorption of mainly organic molecules and biomolecules (e.g., proteins, carbohydrates), forming a conditioning film. This provides some of the necessary nutrients and is thus followed by the colonisation of the surface by a variety of unicellular organisms (bacteria, diatoms). As their settlement mechanism, these organisms utilise a range of polymeric secretions known as extracellular polymer substances (EPS) which will help them adhere onto the surface and will act as the binder of the so called biofilm. This process is referred to as microfouling, and the related microorganisms as microfoulers (with dimensions typically up to 100 µm). Biofilm formation is then followed by the recruitment of macroscopically visible macrofoulers, either “soft” (e.g., algae, seaweed) or “hard” (e.g., barnacles, mussels), with the intermediate attachment of spores for plants and larvae for invertebrate animal species. The timeline for the formation of the conditioning film is considered to be minutes, with biofilm formation occurring within hours. Macrofouling then develops as a matter of days.

Despite the apparently linear evolution, marine biofouling is a highly dynamic phenomenon: for example, spores and larvae can attach onto substrates also in the absence of a biofilm [1], and biofilm presence has been reported to either promote, inhibit or not affect the attachment of macrofoulers [1,17]. This is indicative of the even more striking characteristic of marine biofouling: diversity.

The remarkable variety of potential micro- and macrofoulers in marine ecosystems in different geographical locations is promoted and affected by a very wide range of factors [16,17] such as: temperature, nutrients, sunlight, salinity/ionic strength, pH and dissolved gases. The vast number of fouling species is then accompanied by a plethora of adopted adhesion mechanisms, as well as a dependence on existing organisms and biofilms on the substrate of interest. For example, barnacles employ hydrophobic proteins (collectively known as barnacle cement) for their attachment and utilise a transglutaminase-mediated cross-linking mechanism which resembles blood clotting [18]. Diatoms, on the other hand, use hydrophilic polysaccharide secretions for their adhesion [5,10]. Mussels—which are a focal species in this review—have one of the most well-studied anchoring system in the marine environment, employing a range of peptides with highly specialised and sophisticated

design (known as mussel adhesive proteins, MAPs, or mussel foot proteins, MFPs) in the adhesive plaque as well as the byssus. The MAPs located at the interface of the adhesive plaque with the substrate are particularly rich in L-3,4-dihydroxyphenylalanine (L-DOPA) sequences, which is the key carrier moiety of the 3,4-dihydroxyphenyl (catechol) motif responsible for the mussels' universal underwater adhesion [19–21].

As a result, the attributes which an antifouling coating would need to exhibit in order to be effective under such variable environmental conditions and attachment motifs are often contradictory (e.g., resist hydrophilic and hydrophobic bioadhesives) and highlight the need for smart and adaptable systems.

However, nature has already shown the way in this respect as well, with some of the most advanced defense systems against biofouling demonstrated by other marine organisms. Several sea organisms (e.g., seaweed, sponges, algae, eelgrass) produce small molecules (e.g., 1,1,3,3-tetrabromo-2-heptanone [22], zosteric acid [23]) as secondary metabolites which disrupt the attachment, growth and/or density of bacterial biofilms. Pyrrole-imidazole alkaloids, PIAs [24–26] refer to a family of naturally occurring alkaloids, with oroidin (a dibromopyrrole-2-aminoimidazole) being the first discovered [24] and most well-known member of the family. The PIAs are found in the *Agelas* sponges, and are one of the widely studied family of marine metabolites with a broad range of bacterial anti-biofilm activity. However, not only small molecules have been employed by marine species in their defense against foulers: fucoidan [27–31] refers to a family of sulfated polysaccharides comprising a significant percentage of L-fucose (6-deoxy-L-galactose) repeat units, together with other residues (e.g., glucuronic acid). Fucoidans are found in brown seaweed cell walls as well as in sea urchins and sea cucumbers, and their exact structure varies between species. Fucoidans exhibit a very broad range of bioactivity [27,31] including protein repellency [30] and antimicrobial/antibiofilm [29], antifungal, anticoagulant and anti-inflammatory properties.

Apart from changing their surface chemistry to hinder biofouling, marine organisms also employ an astonishing range of surface topographies and textures for the same purpose [1,7,11]. The surface structural features of the outer shell of different mollusks, mussels and crabs [7] have been highlighted for their micrometric features (e.g., ridges or spikes) and their perceived action as a deterrent against fouling. It has been postulated that settlement of foulers is hindered when the domain size of the structural features is smaller than the size of the foulers themselves [11], or of the organs/means the foulers would utilise to probe the surface for attachment (e.g., antennae [1]). Wetting of a surface is also affected by the presence of surface features and their roughness. It appears, however, that the synergy between topography and surface chemistry is critical for successful antifouling due to the large variety of possible fouling species [11]. In the case of marine mammals (dolphins, whales) and some fish (sharks, rays), the presence of patterned skin with hierarchical micro- and nano-topographical features (e.g., diamond-shaped platelets with longitudinal ribs [1,7,11]) has been shown to improve their hydrodynamic performance and simultaneously reduce fouling. It has to be noted here that hydrodynamic conditions pose another great challenge to successful marine antifouling solutions and specifically to biomimetic approaches, as different marine species operate under largely varied hydrodynamic environments (e.g., Reynolds numbers in the order of  $10^{-5}$ – $10^{-1}$  for microfoulers compared to  $10^5$ – $10^7$  for large fish/marine mammals and man-made vessels [11], Figure 1). Therefore, solutions that are adopted by marine species at low Reynolds numbers and on small surface areas (e.g., ridges on mollusk and mussel outer shell) may not be equally successful for fast-moving vessels. Equally, while high velocities usually facilitate the detachment of macrofoulers from low surface energy surfaces (e.g., in foul-release coatings), the same is not necessarily true for microfoulers (e.g., diatoms) [11].

As a result, a number of efforts to mimic successful natural antifouling topographies have been made, with polymeric replicates of the shark skin textured surface patterns commercialised in the form of an adhesively backed film [32]. One of the most promising biomimetic approaches towards a commercially available non-biocidal anti-adhesive marine antifouling coating (and hence of interest here) has gained inspiration from the slippery peristome (“lip” around the plant’s digestive sack)

surface of the carnivorous *Nepenthes* pitcher plant [33]. The extremely anti-adhesive behavior of the peristome is a combination of complete wetting (by either rainwater or nectar) and underlying anisotropic surface topography, comprising a series of radial ridges forming a “downward staircase” leading to the digestion sack of the plant. The stable liquid boundary layer present on the peristome is the key to low friction and hence inability of insects to walk away from the peristome.

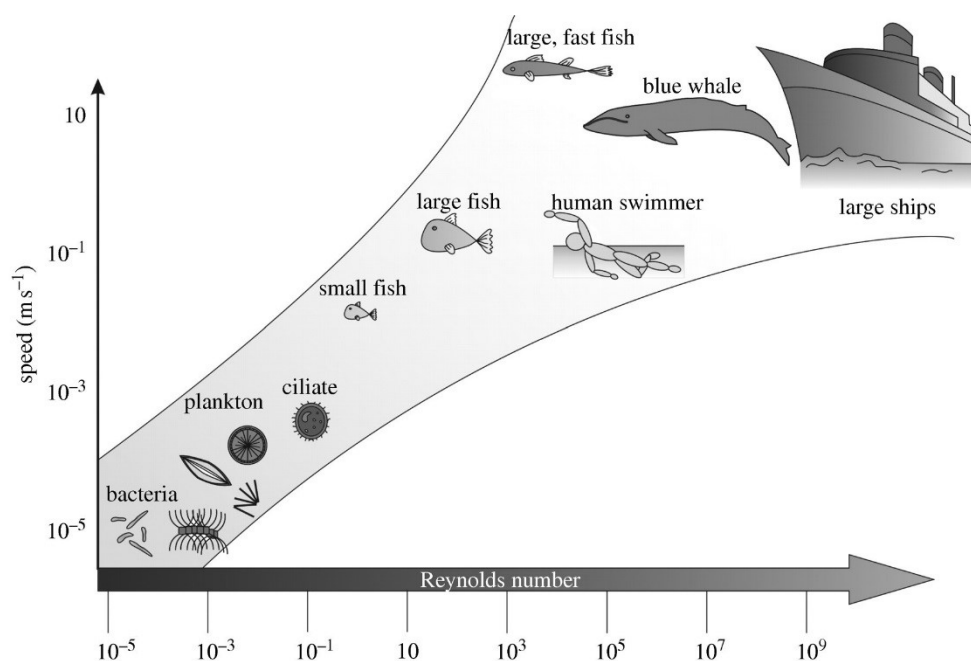


**Figure 1.** Reynolds numbers for various marine biofoulers and other relevant species and systems (e.g., fish, large mammals, ships). Reproduced from reference [11], with permission. Copyright (2010) The Royal Society.

The stable liquid interface principle has been exploited by Aizenberg and co-workers [34–36] in a biomimetic materials system that utilises a patterned porous substrate to establish a liquid surface layer and thus create a stable liquid/air interface (slippery liquid-infused porous surfaces, SLIPS).

It is claimed that the molecularly dynamic nature of the liquid layer (in contrast to traditional solid-state antifouling coating approaches) is beneficial in the direction of hindering any permanent interaction between a bioadhesive from a fouling species and the surface—in contrast with a solid coating, which—even if highly antifouling—will eventually become colonised to some extent. The direct approach has been to select microporous substrates (e.g., Teflon membranes [34], poly(dimethylsiloxane), PDMS [34–36]) and infuse with chemically compatible liquids (e.g., poly(perfluoro ether)s for Teflon, silicon oil for PDMS). However, surface nanostructuring and/or surface chemical functionalization has also allowed for the matching of chemically dissimilar components (e.g., a nanostructured PDMS surface infused with poly(perfluoro ether)s [34]). A visual summary of the SLIPS approach is shown in Figure 2. Interestingly, in a combined laboratory and field study using live Asian green mussels *Perna viridis* [36], a PDMS coating infused with silicon oil has been shown to not only reduce the number of mussels attached per unit surface (number of adhesive plaques formed, see Section 3), but to additionally diminish the adhesive strength of those attached plaques ( $3.4 \pm 2.0$  kPa for the lubricant-infused PDMS): by one order of magnitude compared to control untreated PDMS, and at least by half compared to state-of-the-art commercially available non-fouling silicone paint for ship hulls. The simplicity, efficacy, durability and self-replenishing capacity (when removed, the surface layer of the lubricant can be replaced from liquid absorbed further in the pores of the substrate diffusing to the interface [35]) of this approach has led to a commercially available SLIPS marine antifouling paint [37].

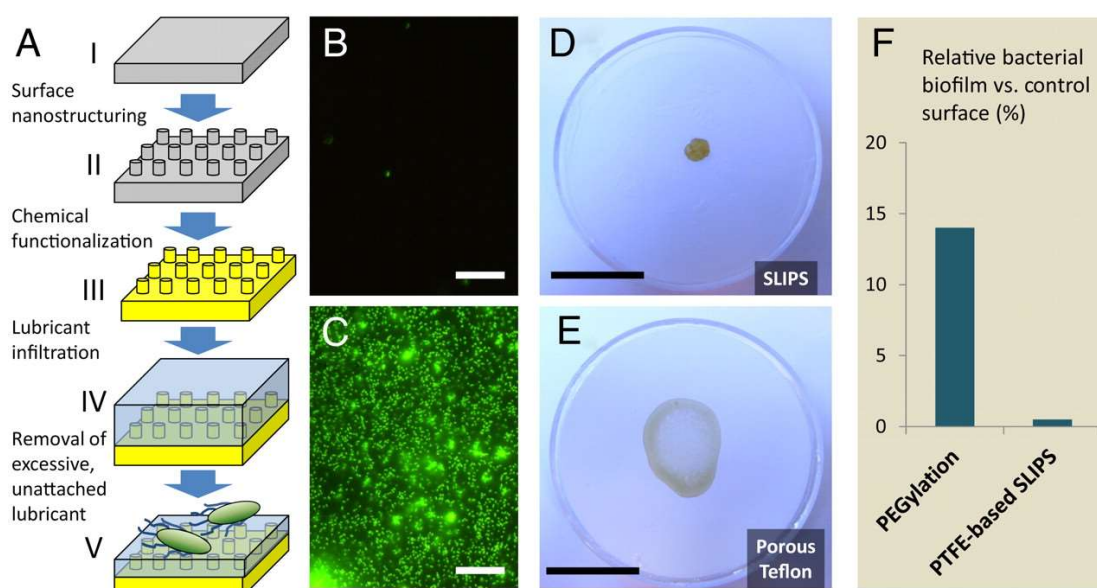


**Figure 2.** Visual summary of the slippery liquid-infused porous surfaces (SLIPS) approach. (A): SLIPS fabrication flow chart; (B,C): fluorescence micrographs of attached *P. aeruginosa* biofilm on SLIPS (B) and superhydrophobic Teflon (C) under the same conditions; (D,E): wetting characteristics of a drop-cast biofilm of *P. aeruginosa* on SLIPS (D; limited wetting, loosely attached and easily removable) and superhydrophobic Teflon (E; complete wetting, high adhesion); (F): comparison of biofilm attachment on a SLIPS surface (after 7 days) and on a PEGylated surface (after only 5 h), showing a 30-fold increase in anti-biofilm capacity for SLIPS against a gold-standard antifouling material. Reproduced from reference [34], with permission.

### 3. Mussel-Inspired Synthetic Polymers and Catechol-Mediated Adhesion

#### 3.1. Mussel Biology, Biochemistry and Mechanics of Adhesion

As demonstrated at the end of Section 2 [36], mussels are one of the most prolific macrofoulers found in the marine environment. Their ability to opportunistically adhere onto any surface available and remain attached despite the many challenges posed by the marine environment (temperature, salinity, biofilm-colonised surfaces, waves and currents) is key to their survival and development during their life cycle.

Across their different genera, mussels have developed a unique tethering and shock-absorbing system, universally known as the mussel byssus [20,38,39] (Figure 3).

The byssus comprises four distinct regions which differ in terms of chemical composition, microstructure and morphology - and hence mechanical properties [20,38,39]: the stem, the proximal part of the byssal thread (corrugated and very highly extensible), the distal part of the byssal thread (straight and stiffer than the proximal, yet still significantly extensible) and the adhesive plaque (in contact with the substrate). The generation and release of the byssus takes place within and from a dedicated organ known as the mussel foot: a tongue-like element with an internal structure comprising amongst other features a longitudinal tubular channel (ventral groove). The foot itself has also a sensory role, as it probes the surface around the animal in order to select the exact place of attachment. When this happens, the foot attaches onto the specific area and a mixture of proteinaceous substances is secreted and shaped via contractions into the byssus with its four compartments. The process lasts just a few minutes and has been claimed to resemble several industrial polymer processing techniques [20,38–41]: extrusion [41] and injection moulding of collagenous liquid crystals [39] for the byssal thread, sizing for the deposition of a protective coating on both thread and plaque [41], and reactive injection moulding for the formation of the adhesive plaque [20,38–41]. The microenvironment within this “multi-processing chamber”, and specifically for plaque formation, is very carefully controlled in terms

of pH, ionic strength and redox conditions in order to achieve optimal results with respect to adhesion of the plaque and mechanical performance of the byssal thread [39].

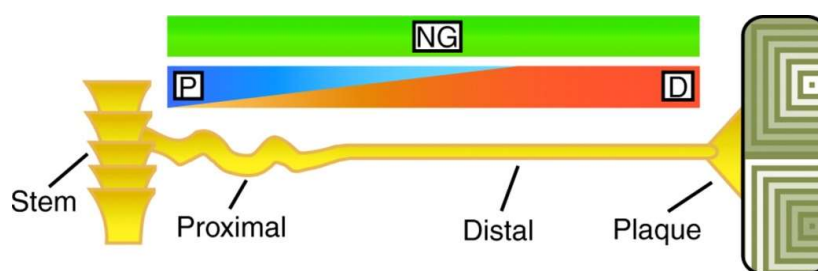
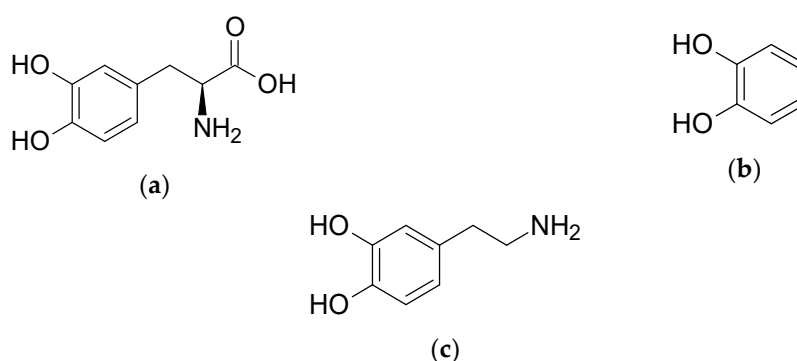


**Figure 3.** Schematic representation of the mussel byssus tethering system. P, D and NG refer to the different prepolymerised collagen (preCol) variants and their gradient distribution along the thread (see reference [38]). Reproduced with permission from reference [38]. Copyright (2007) The Company of Biologists.

Since the pioneering work by Herbert Waite and collaborators [15,42], it has been the genus *Mytilus* (mytilids) that has been extensively studied with respect to the exact composition of the four byssal regions and the potential interactions and synergies between the building blocks in each region. Up to 30 different proteins have been identified in the byssus of mytilids [19,20,39], with only five proteins found exclusively in the adhesive plaque: MFP-2 to MFP-6. There is also MFP-1 which is a key component of a protective coating on the byssal threads and the plaque, while the byssal threads are mainly composed of a range of collagenous proteins (known as prepolymerised collagens, preCols, and thread matrix proteins, tmp). While MFP-1 to MFP-6 vary greatly in their amino acid sequences, repeat number, molecular weight and charge density, there is an overarching common feature in that all MFPs contain sequences from the  $\alpha$ -amino acid derivative L-3,4-dihydroxyphenylalanine (L-DOPA, Scheme 1), ranging from 2% to 30% mol [19,20,39,43]. L-DOPA is a multifunctional compound with three chemical groups (amine, carboxyl, *o*-bisphenol) and especially until the early reports [15,42] it had not been frequently encountered in naturally occurring proteins. As a result, its abundant presence in MFPs attracted considerable interest, and specifically the 3,4-dihydroxyphenyl (catechol) moiety has since been consistently linked with the adhesive, cohesive and self-healing properties of MFPs.



**Scheme 1.** Structures of (a) L-DOPA (L-3,4-dihydroxyphenylalanine); (b) catechol (1,2-bisphenol); and (c) dopamine (produced from the decarboxylation of L-DOPA).

However, a high concentration of catechols in a synthetic polymer MFP analogue will not necessarily and linearly result in increased levels of adhesion—particularly underwater [39]. Although L-DOPA and catechol are indeed heavily implicated in a number of byssal operations using covalent and non-covalent mechanisms (including protein-protein interactions), the level of microenvironment control imposed by the mussel during the formation of the byssus is very difficult to replicate with an underwater adhesive delivery system [39]. Still, the catechol moiety is one of the most

versatile molecular design tools for achieving good performance and simultaneous control on adhesion/cohesion/self-healing in synthetic adhesives and coatings [44]. Table 1 summarises some of the key characteristics of plaque MFPs.

**Table 1.** Main characteristics of mussel foot proteins (MFPs) in mytilids [19,20,39,43].

Protein	Molar Mass (kDa)	L-DOPA Content (mol%)	Location in Byssus	Role
MFP-1	90–130 <sup>1</sup>	15	Byssal thread cuticle	Main cuticle component
MFP-2	45	5	Bulk of plaque	Main building block of bulk plaque
MFP-3	6	20	Plaque-substrate interface	Plaque adhesive
MFP-4	90	2	Proximal end of plaque	Linkage to preCols from byssal thread
MFP-5	9	30	Plaque-substrate interface	Plaque adhesive
MFP-6	12	3–5	Plaque-substrate interface	Sacrificial antioxidant to maintain MFP-3/MFP-5 adhesion potency

<sup>1</sup> Reported variations between different mytilids.

Common features amongst all MFPs include the presence of L-DOPA sequences (up to 30% for MFP-5 which is situated at the substrate–plaque interface) and a high content of cationic aminoacids (e.g., lysine, histidine, arginine), i.e., a basic isoelectric point, pI [19,20,39,43]. The presence of L-DOPA has been linked with strong interfacial adhesion as well as curing/cohesion of the plaque and the byssus, depending on a number of factors (pH, presence of metal ions, other reactants e.g., amines and thiols). The exact adhesive function of the catechol moiety with the related chemistry and specific covalent and non-covalent bonds involved in adhesion/cohesion/self-healing will be discussed in detail in Section 3.2.

It is MFP-3, MFP-5 and MFP-6 that are present at the plaque-substrate interface and arguably directly involved in mussel adhesion. However, it is MFP-3 and MFP-5 with high mol% in L-DOPA (20% and 30%, respectively) that indeed adsorb on the substrate via their abundant catecholic hydroxyls, whereas MFP-6 with decreased L-DOPA (3–5 mol%) and increased cysteine (11 mol%) content acts as an antioxidant and protects the MFP-3/MFP-5 catechols from oxidation to *ortho*-quinone [43,45,46], which is promoted in the mildly alkaline seawater pH range (7.5–8.4). This protection is accomplished by a sophisticated range of reactions [43–47], including oxidation of the cysteine thiol group to disulfide, sacrificial MFP-6 catechol oxidation (rather than those of MFP-3/MFP-5) to quinone and the formation of various S-cysteinyl-catechol adducts [44,47] from a Michael-type addition reaction of the thiol moiety onto (mainly) the 5- and/or 2- position of the quinone ring (effectively achieving quinone reduction and cross-linking simultaneously). These reactions are detailed in Section 3.2.2.

In terms of the plaque microstructure, scanning electron microscopy (SEM) studies [20,48] suggested a porous structure (approximately 40% porosity [20]) resembling an open-cell structural foam with a combination of a dense meshwork with large interpenetrating pores [48]. Interestingly, the plaque appeared to resist treatment with a known protein denaturation agent (6M guanidine hydrochloride), indicating significant cross-linking [48] of the plaque proteins.

While L-DOPA is abundantly present in the plaque, its role and contribution extends further than adhesion at the plaque-substrate interface. For example, a small number of L-DOPA residues (between 2–4 [38]) is found at the C- and N-termini of the prepolymerised collagens of the byssal threads [38,40,49,50], where they are thought to contribute to chain-end-mediated covalent cross-linking of separate preCols [38] via a 5,5'-biscatechol adduct [51]. The termini as well as the adjacent flanking domains are also rich in histidine residues, which (as the catechol moiety in L-DOPA) can form coordination complexes with metal ions and thus contribute to a reversible domain unfolding and self-healing process of the collagen-rich byssal threads [38,49,50], thereby contributing to the high extensibility observed in the distal thread region.

Furthermore, L-DOPA appears to play a protagonist role in the protective coating (cuticle) on the byssal threads [52–56], through its presence in MFP-1. The latter is the only MFP and the majority component of the cuticle, together with small amounts of metal ions (e.g., iron, calcium) and fatty acids. The main function of the 2–5  $\mu\text{m}$  thick sheath is to protect the byssal threads from abrasive damage, and hence exhibits 5-fold increased hardness and 3-fold increased stiffness [53,55] compared to the underlying preCol fibres. Remarkably, it also shows similar strain at break values to those of the collagenous threads, spanning amongst different mytilids between 70–120% of the original length at failure [53,55]. This unique combination of otherwise mutually exclusive material properties is attributed to the cuticle microstructure, which resembles a particle-reinforced polymer-matrix composite [54,56]: the dispersed phase (at approximately 50% volume fraction) consists of spherical/ellipsoidal domains (granules) which are distributed in a continuous MFP-1 matrix. Raman spectroscopy [56] suggested that the granules correspond to areas of high density of  $\text{Fe}^{3+}$ –catechol complexes. After a certain level of elongation at low strains, the granules cease to change their aspect ratio at moderate strains and begin to behave as load-bearing stiff filler particles—and potentially as microcrack-arresting features [52] of damage observed in the matrix, thereby preventing catastrophic failure and increasing the overall extensibility of the cuticle. The species that showed smaller granule diameters (200 nm for *Mytilus californianus* compared to 800–1000 nm for other mytilids [55]) also appear to reach the higher end of the ultimate strain range; unsurprisingly, mussels that—unlike the intertidal mytilids—inhabit subtidal, calm waters (e.g., *Perna canaliculus*) only reach 30% extensibility and do not exhibit any microphase separation in their byssal cuticle [52].

### 3.2. L-DOPA and Catechol Chemistry: Adhesion, Cohesion, Self-Healing and Synthetic Mussel Foot Protein (MFP) Analogues

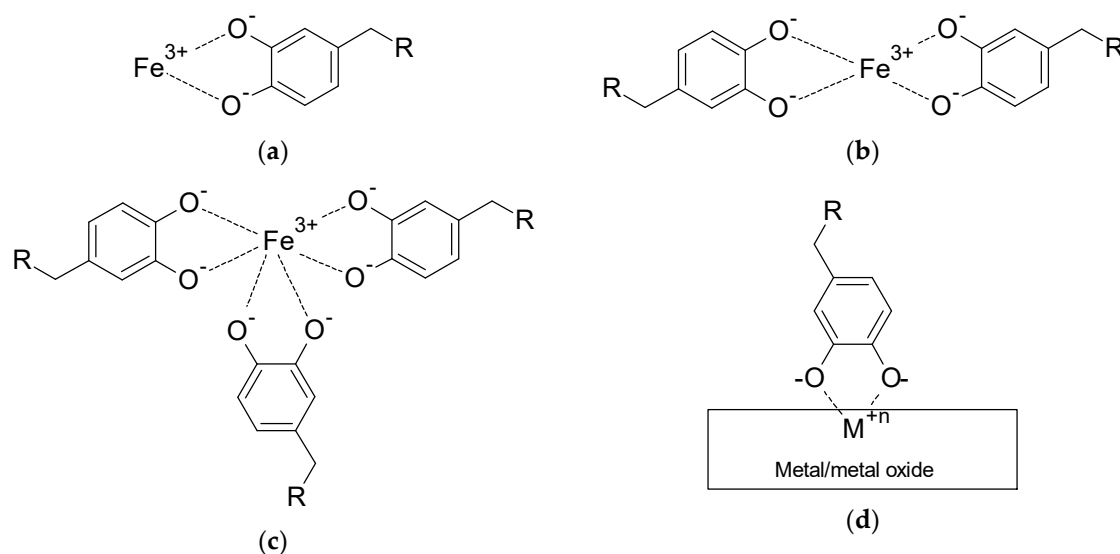
As mentioned several times in this review, the presence of L-DOPA in MFP sequences has been linked from early on with the advanced adhesive, cohesive and self-healing properties of the mussel byssus [15,19–21,42]. The significance of the catechol moiety in L-DOPA and its versatile chemistry in relation to adhesion as well as cohesion and self-healing has been in turn identified and reviewed in detail [19,20,44]. In this section, the most relevant catechol chemistries (covalent and non-covalent) will be summarised, and an overview of the key synthetic MFP analogues will be provided.

#### 3.2.1. Adhesion: Metal Coordination and Catechol Oxidation

The strong adhesion of catechol-bearing moieties on a range of metal and ceramic/metal oxide surfaces (demonstrated by mussels successfully adhering on wave-swept rocks) is the outcome of a delicate balance between (i) metal coordination capacity of the catecholic hydroxyl groups, and (ii) oxidation of catechol to semi-*ortho*-quinone/*ortho*-quinone [19,20,57].

Complex formation of catecholate ligands with a variety of metal ions (e.g.,  $\text{Fe}^{3+}$ ,  $\text{V}^{3+}$ ,  $\text{Mn}^{3+}$ ,  $\text{Ti}^{4+}$ ,  $\text{Cu}^{2+}$ ,  $\text{Co}^{2+}$ ,  $\text{Ni}^{2+}$ ) in solution has been documented using small molecules (catechol itself, and tiron: 4,5-dihydroxy-1,3-benzenedisulfonic acid disodium salt) [58], short L-DOPA-containing oligopeptides (e.g., alanine-L-DOPA-threonine-proline) as MFP mimics prepared by standard solid-phase peptide synthesis [59], and uncured mussel foot protein extract removed from *Mytilus edulis* [60]. The two former studies focused on ultraviolet–visible (UV-Vis) absorption of aqueous solutions and relevant complex formation/binding constants, and revealed that the complex stoichiometry (mono-, bis- and tris-catecholates) and the spectroscopic and binding properties of the formed complexes were in general similar between catechol itself and the oligopeptide MFP mimics [59]. The latter study [60] focused on the mechanical properties of the formed crosslinked network after mixing the MFP extract with various amounts of metal ions. The mechanical strength of the  $\text{Fe}^{3+}$ –catechol gels was at least five times higher compared to all other metal ions tested, indicating the particularly high affinity of  $\text{Fe}^{3+}$  for the catecholic hydroxyl ligands. These observations tie in with the previously mentioned works on the cuticle of the mussel byssus [52–56] where bis- and tris-  $\text{Fe}^{3+}$ –catecholate complexes were identified by Raman spectroscopy as the crosslinking mechanism. Wilker et al. [60] also make the point of the very

high trace metal content (e.g., Mn, Fe, Cu, Zn) found in mussels compared to average concentrations in open ocean. Scheme 2a–c shows the structure of mono-, bis- and tri-  $\text{Fe}^{3+}$  catecholates.



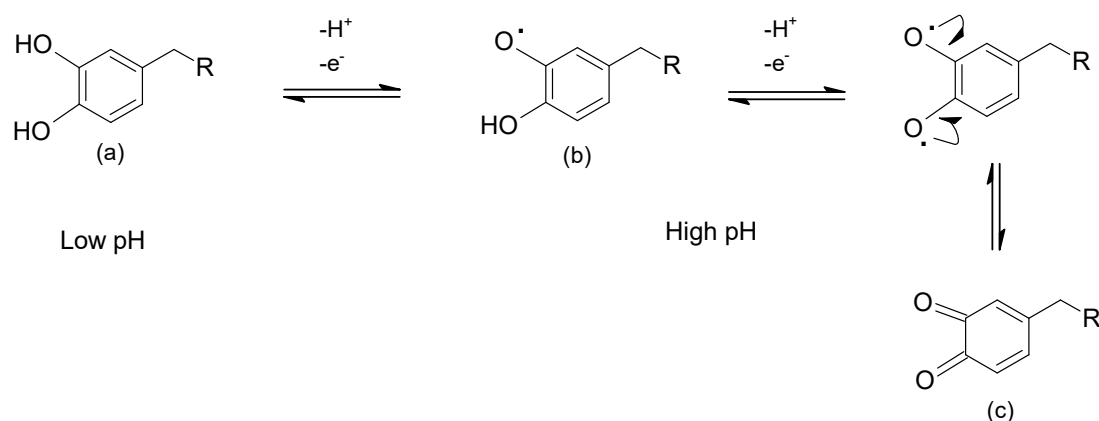
**Scheme 2.** Structures of generic metal–catechol complexes: (a)  $\text{Fe}^{3+}$  mono-catecholate; (b)  $\text{Fe}^{3+}$  bis-catecholate; (c)  $\text{Fe}^{3+}$  tris-catecholate; (d) generalised adsorption of catechol-bearing molecule on metal or metal oxide surface, via the formation of a mono-catecholate complex with surface metal ions.

Adsorption of catechol-functionalised molecules on metal and metal oxide surfaces follows a similar mechanism, where the bisphenol moieties form mono-catecholate complexes with metal ions on the substrate's surface [20,57,61]. Scheme 2d provides a generalised depiction of surface adsorption of catechol-bearing species. It is clear that the nature of the R-group will influence the exact adsorption geometry and surface coverage with any steric or intermolecular effects, as well as ultimately the adhesion strength and the quality of the formed adsorbate layer. For example, the presence of amide-bond-induced hydrogen bonding between the chains of *N*-stearoyldopamine (where  $\text{R} = -\text{NHCO}(\text{CH}_2)_{16}\text{CH}_3$ , as per Scheme 2d) adsorbed on gold surfaces results in a tilted geometry and a more robust monolayer compared to 4-stearylcatechol, where  $\text{R} = -(\text{CH}_2)_{15}\text{CH}_3$  [62].

As with metal ion–catechol complex formation in solution, surface adsorption is reversible; and particularly in the case of underwater adhesion for mussels, pH dependent. This is because catechol oxidation to its semi-quinone and quinone forms is promoted under high pH conditions, whereas reduction of quinone back to catechol is observed at low pH values. Scheme 3 shows the catechol/*o*-quinone equilibrium reaction.

In related single-molecule studies [63], atomic force microscopy (AFM) cantilever tips were functionalised with a single catechol-terminated PEG chain and probed different substrates (including Ti and an amine-modified silicon wafer to simulate tissue) under different pH conditions to measure adhesive force. At pH 7, catechol is predominantly present in its reduced bisphenol form and hence a reproducible (observed in populations of more than 100 tip contacts), unimodal pull-off force profile was obtained with a strong mean adhesive force of 805 pN. At pH 9.7, it is the quinone that prevails with some unoxidised catechol still present. As a result, a bimodal pull-off force profile was recorded: a low-force population (mean of 180 pN, 74% of tip contacts) corresponding to quinone, and a high-force population (mean of 740 pN, 26% of tip contacts) corresponding to catechol.

At pH 8.3, one would expect that the presence of unoxidised free catechol would increase compared to pH 9.7 with an accompanying effect in adhesive strength. Indeed, this was the case: with 62% of tip contacts in the high-force population, and 38% in the low-force population.



**Scheme 3.** pH-dependent oxidation of catechol-bearing species (a) to semi-*o*-quinone (b), one-electron oxidation; and *o*-quinone (c), two-electron oxidation.

This is not to imply that the presence of quinone moieties cannot contribute towards strong interfacial adhesion; however, this would not be via a metal chelation mechanism, but through covalent interactions. For organic/biological substrates (e.g., tissue) in particular, the highly reactive quinones undergo reactions with nucleophiles usually present on such surfaces (e.g., amines, thiols) leading to Michael-type adducts (with either  $-\text{NH}_2$  or  $-\text{SH}$ ) or imine bond formation (with  $-\text{NH}_2$ ) [19,20,44,57,63]. A silicon wafer which was surface-functionalised with amine groups was employed to mimic a tissue surface in the single-molecule AFM study [63] and was tested in pH 9.7 (where quinone is predominantly present), and an even higher pull-off force of 2200 pN was observed. This adhesion was not reproducible as in the previous cases: it was observed up to the 78th tip contact, and no detectable adhesion was noted for another 800 tip approaches. This is consistent with the rupture of a covalent bond rather than with the reversible metal-catechol interaction, and the authors [63] suggested the formation of a Michael-type adduct between amine surface groups and the quinone ring. The high reactivity of quinones is further exploited in terms of enhancing cohesion with nucleophilic additions and substitutions, as well as with aryl coupling reactions and self-oligomerisation (see Sections 3.2.2 and 3.2.4).

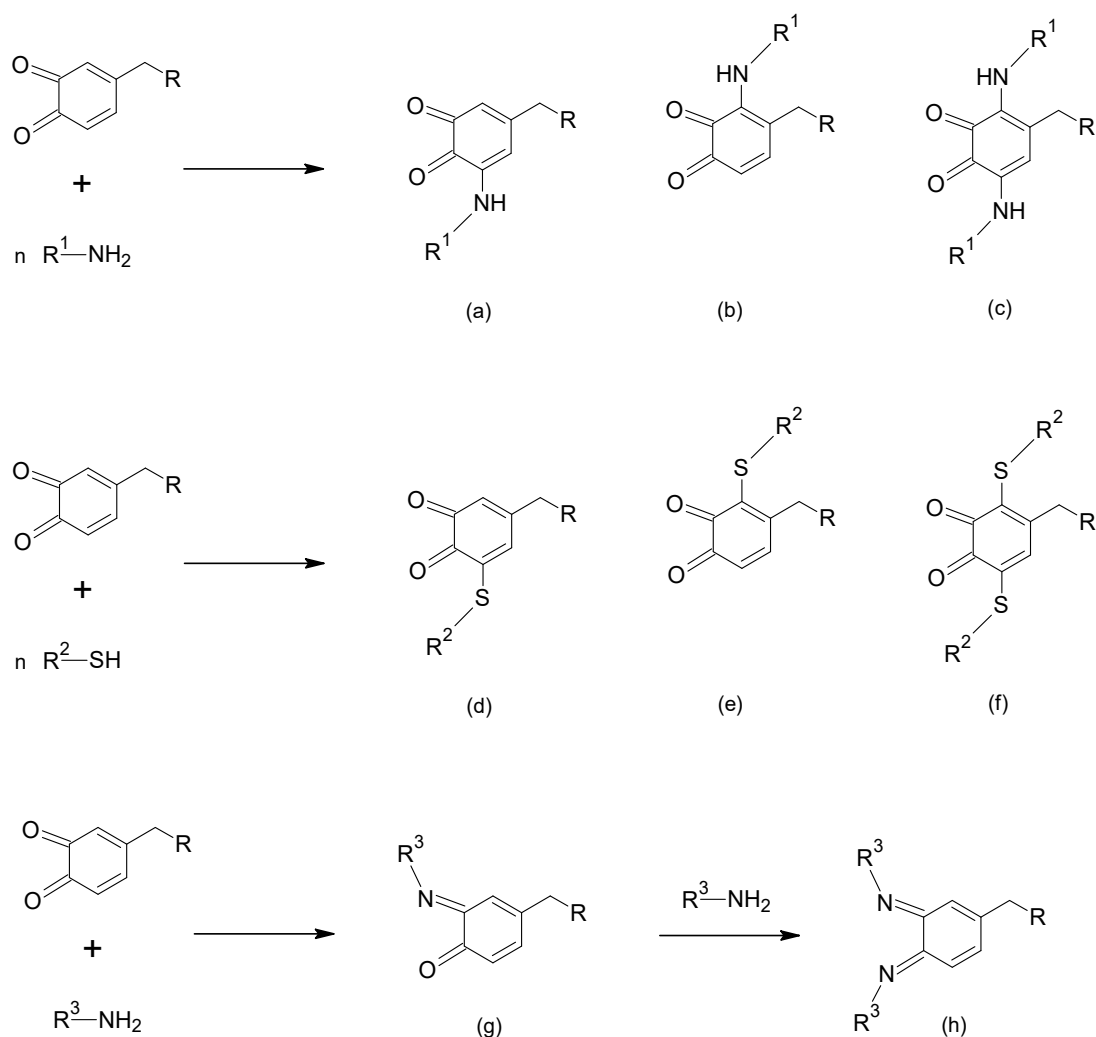
Combining the above discussion and Schemes 2 and 3, it is evident that mono-catecholate complexes which mediate surface adhesion would be favoured at low pH/catechol prevalence, whereas bis- and tris-catecholate complexes would be favoured at high pH/quinone prevalence and contribute towards cohesion rather than adhesion (e.g., in the MFP-1 rich cuticle of the byssus [52–56]). As a result, the pH of the local area where plaque formation occurs (known as the distal depression [39]) is carefully maintained in the acidic pH range by the mussel in order to promote adhesion, whilst the surrounding seawater environment remains in slightly alkaline pH values and hence promotes processes favoured under these conditions, e.g., reinforcement of protective cuticle in mussel byssus with  $\text{Fe}^{3+}$ /tris-catecholate rich inclusions [56]. It has been suggested [64] that, as  $\text{Fe}^{3+}$  has very limited solubility in neutral/basic environments, MFP-1 forms mono-catecholate “pre-complexes” with  $\text{Fe}^{3+}$  during byssus formation under the acidic conditions of the ventral groove; these pre-bound entities would then spontaneously convert to bis- and tris-catecholates upon exposure to seawater—thereby contributing towards cohesion and self-healing of the unique byssal cuticle.

### 3.2.2. Cohesion: Covalent Interactions

Both catechols and *o*-quinones exhibit a significant range of covalent reactions they participate in, with the *o*-quinone generally considered a more reactive moiety. In this section, we review some of the related covalent chemistries which have been mentioned in Section 3.1. Oxidation of catechol to *o*-quinone has already been covered in Section 3.2.1.

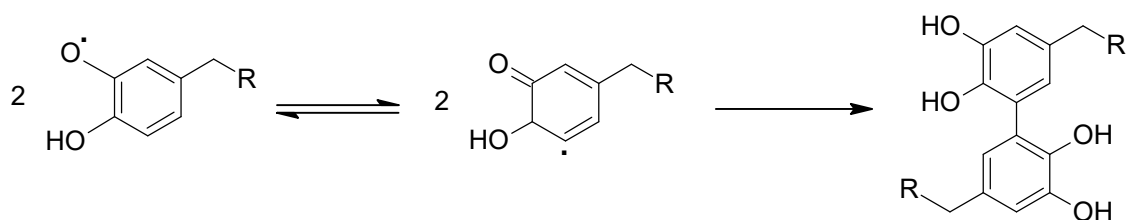
The presence of the two carbonyl groups on the *o*-quinone ring provides carbonyl centres for imine formation, and allows the ring to act as Michael acceptor in reaction with suitable nucleophiles such as

amines, imidazoles (including histidine) and thiols [44]. Imine formation can take place on one or both carbonyls, and nucleophilic addition in the 2-, 5- or both ring positions [44]. Basicity/nucleophilicity of the amine/thiol reagent and pH are common factors affecting both imine formation and Michael-type addition reactions [44], along with steric and electronic substituent effects. The 5- position seems to be the preferred one in the Michael-type reaction, presumably due to its less congested configuration. Apart from the role of the Michael-type reaction in the antioxidant activity of MFP-6 described in Section 3.1 [43–47] and a possible covalent contribution to interfacial adhesion [19,20,57,63], these reactions provide a covalent route to cohesive strength enhancement. Scheme 4 depicts generic reaction schemes for imine formation and Michael-type addition with amines and thiols on an *o*-quinone substrate.



**Scheme 4.** Generic reaction schemes of *o*-quinone species with nucleophiles. Top and middle: Michael-type addition with amines (**top**) and thiols (**middle**), with 5-substituted dominant products (**a,d**, respectively) depicted together with minority products substituted at the 2-position (**b,e**) and the 2,5-bis-variant (**c,f**). Bottom: Schiff base (imine) formation by reaction with amines, with mono- (**g**) and bis-imine (**h**) products.

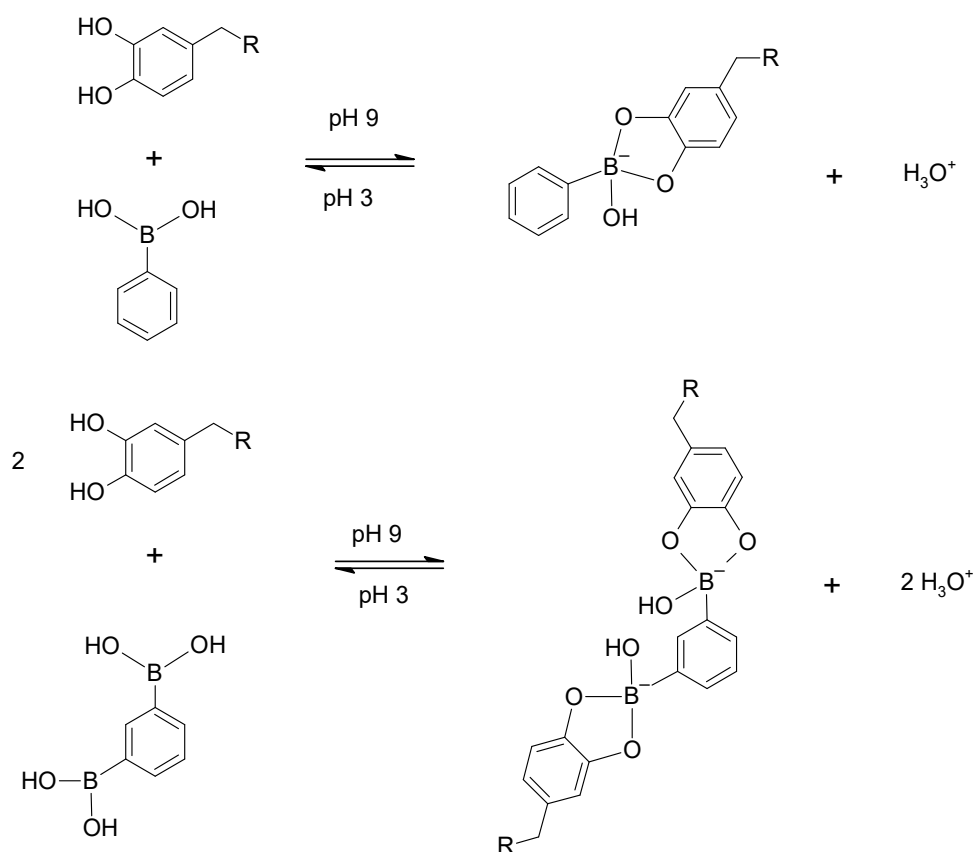
Another route to covalent crosslinking (apart from the adhesive plaque), which has been identified as part of the highlighted L-DOPA contribution in the mussel byssal processes is in chain-end-mediated covalent cross-linking of separate preCols [38] via a 5,5'-biscatechol adduct [51]. This involves oxidative aryl coupling between two semi-*o*-quinone radical moieties [44] and is shown in Scheme 5.



**Scheme 5.** Generic reaction scheme for aryl coupling of semi-*o*-quinone species (see Scheme 3b) and formation of a 5,5'-biaryl adduct (termed as 5,5'-diDOPA in [38,51]).

It has to be noted here that the oxidative activation of the catechol ring to its *o*-quinone counterpart is directly linked to some of the most well-known relevant synthetic polymers, which stem from the oxidative self-polymerisation of catecholamine structures, with dopamine (Scheme 1) and polydopamine (PDA) formation being the first reported and most prominent example [65]. Polycatecholamines and polydopamine are reviewed further in Section 3.2.4.

A last covalent reaction of the catechol hydroxyls which has been neatly exploited in mussel-inspired pH-responsive hydrogels [66] and smart hydrogel adhesives [67] is the reaction with phenylboronic acids and the reversible formation of borate esters (Scheme 6).



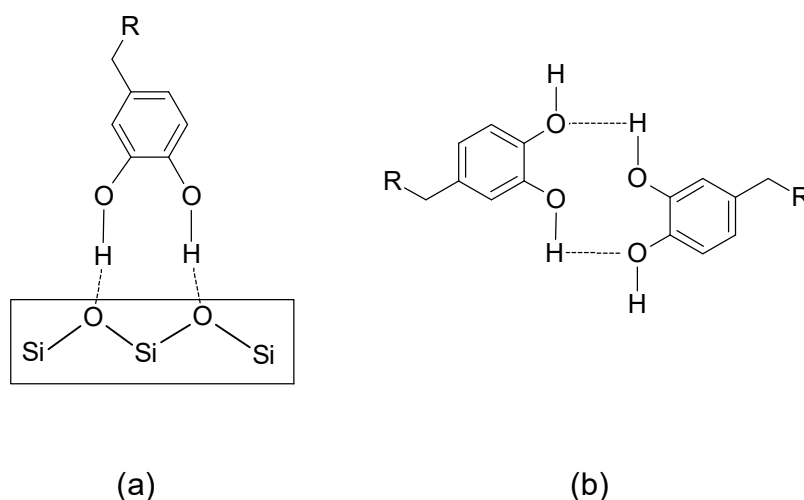
**Scheme 6.** Generic reaction scheme for the formation of borate esters of catechol-functionalised molecules with phenylboronic acid (**top**) and 1,3-benzenebisboronic acid (**bottom**, one example in [66]).

The borate ester formation and stability is dependent on the pH and pK<sub>a</sub> values of the specific diol (here catechol) and boronic acid selected [68,69], and it is for the systems examined [66,67] favoured at higher pH values (pH 9 was selected). This provides a reversible protection strategy against catechol oxidation to quinone in the alkaline pH region, while maintaining free catechol adhesive ability in the

lower pH range (where borate ester formation is limited). It is also a reversible covalent cross-linking approach, yielding hydrogels with enhanced cohesive properties [66,67].

### 3.2.3. Other Non-Covalent Interactions: Adhesion and Self-Healing

Apart from coordination to a metal ion centre and formation of different complexes as described in Scheme 2, the catechol moiety is one of the most versatile in terms of engaging in non-covalent interactions [19,20,57,70]—namely hydrogen bonding,  $\pi$ - $\pi$  stacking, and cation- $\pi$  interactions. The MFPs and their synthetic analogues can furthermore take part in longer-range electrostatic attractions between oppositely charged ions (between cationic aminoacid residues in MFPs and negatively charged surfaces, e.g., lysine and mica, respectively [71]), as well as in hydrophobic interactions between the catechol rings and non-polar residues on surfaces [72]. The versatility of the numerous possible non-covalent interactions stemming from L-DOPA and catechol presence has been identified as a unique contributor in the universal (including underwater) adhesive ability of MFPs and their synthetic counterparts [70,73]. For instance, while Scheme 2d depicts the adhesion mechanism of catechol on metal and metal oxide surfaces, different mechanisms have been identified for the adhesion of extracted MFPs (MFP-1, MFP-3 and MFP-5) on polystyrene and poly(methyl methacrylate), PMMA [73]. Specifically, hydrophobic interactions between the methoxy moiety in the methacrylate group and non-polar segments in the MFPs (e.g., glycine) were proposed to be the reason for the good adhesion of MFPs on PMMA. Similarly, a combination of hydrophobic,  $\pi$ - $\pi$  stacking and cation- $\pi$  interactions seems to be the driving force behind strong MFP adhesion on polystyrene. All these specific MFPs have several cationic aminoacids in their sequence that provide cation centres and can bind to the styrene rings, as well as aromatic (for  $\pi$ - $\pi$  stacking) and hydrophobic side chains from the appropriate aminoacids. In the case of aluminosilicate glass substrates [72,73], it is bidentate hydrogen bonding (Scheme 7) between the catechol hydroxyls (donors) and oxygen atoms in the aluminosilicate network (acceptors) that constitutes the dominant adhesion mechanism, with coordination to the  $Al^{3+}$  centres (if present) also playing a role. As most glasses have surface OH groups as well, these could also contribute in a similar manner (as donor or acceptor).



**Scheme 7.** Generic hydrogen bonding motifs of catechol hydroxyls contributing to adhesion ((a): simplified aluminosilicate substrate) and self-healing ((b): complementary hydrogen bonding with a catechol partner and alternate donor-acceptor function).

These studies [72,73] again highlight that universal MFP adhesion goes beyond the simply elevated presence of L-DOPA residues; while it is catechol coordination and hydrogen bonding that prevail in adhesion to polar and hydrophilic substrates, hydrophobic interactions from other MFP structural features can play the key role when adhering to non-polar (e.g., plastic) substrates.

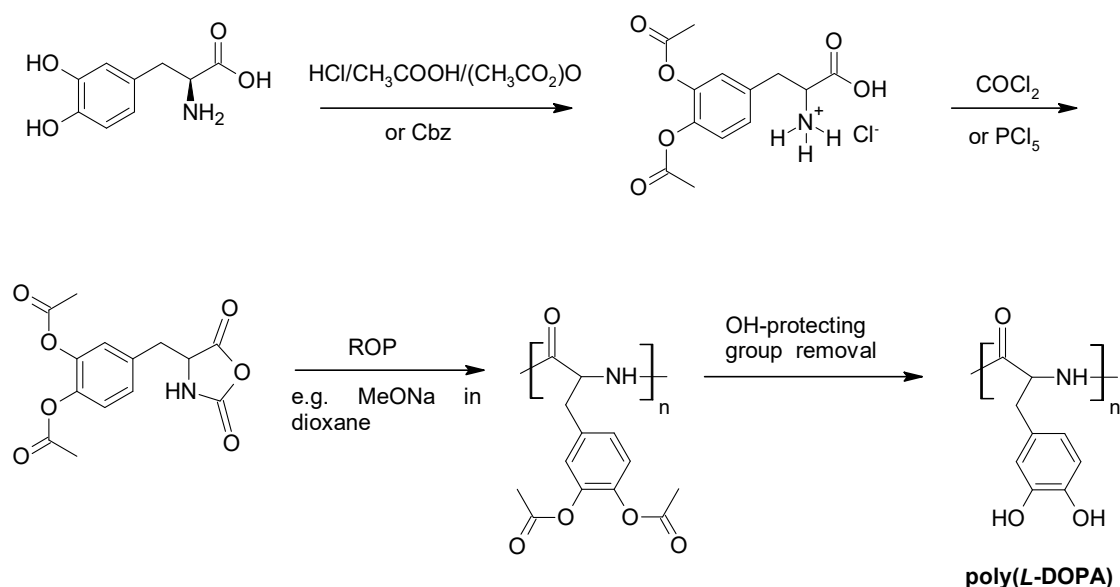
Apart from hydrogen bonding with appropriate oxygen or nitrogen moieties which can contribute towards enhanced surface adhesion on glasses and other polar/hydrophilic substrates, catecholic hydroxyl groups have been suggested to engage in hydrogen bonding with another catechol-bearing molecule [74,75] and provide an alternative metal-free self-healing pathway [74]. Waite and Israelachvili and co-workers [74] have demonstrated this neatly in catechol-bearing methacrylate and methyl methacrylate polymers, in which the catechol hydroxyls were initially protected with triethylsilyl groups. Rods of these polymers were cut by razor blade and the cross-sections were immersed in an aqueous buffer of pH 3, under which the triethylsilyl groups are cleaved and catechol hydroxyls are regenerated. The two cross-sections were then briefly brought in contact under the same pH conditions and the healed materials were tensile-tested. The ultimate tensile strength and the overall performance were at the level of the pristine material, and the interface (where the cross-sections were brought together) had not failed in the vast majority of tested samples. The observed self-healing was attributed to complementary hydrogen bonding (one donor and one acceptor in each molecule) between interfacial catechol moieties, which is in line with the early observed hydrogen-bond-induced dimerisation of catechol in the solid state [76].

Scheme 7 shows different generic catechol hydrogen bonding cases contributing to adhesion and self-healing.

#### 3.2.4. Chronology of Synthetic Mussel Protein Analogues and Mimics: Structures and Synthesis/Modification Strategies

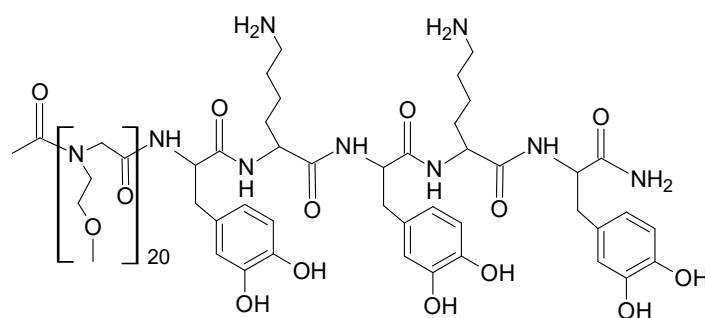
The first efforts to produce synthetic analogues of MFPs were bound to focus on mirroring the early identified mussel protein structures and amino acid sequences, with Yamamoto [77] producing a synthetic version of the MFP-1 repeating decapeptide identified by Waite [42], using amino acid end-group coupling reactions. The produced decapeptide was tested in terms of adhesive properties on iron and alumina substrates with promising results. Interestingly however, the notion of a DOPA-bearing polymer has been researched as early as 1957 [78], with a racemic poly(DL-DOPA) synthesized from its acetylated *N*-carboxyanhydride (NCA) by phosgenation and subsequent ring-opening polymerisation (ROP) and deacetylation, to regenerate the bisphenol functionalities. The optically pure L-DOPA and its synthetic poly( $\alpha$ -amino acid) was first mentioned by Yamamoto et al. [79,80] where the carboxybenzyl (Cbz) protected (both hydroxyl and amine groups) L-DOPA was converted to its NCA using  $\text{PCl}_5$  and subsequently ring-opened-polymerised [79] and converted to poly(L-DOPA) by removing the carboxybenzyl groups [80]. High molecular weight poly(L-DOPA) was reported [81] by a similar route, where the carboxybenzyl group was replaced by acetylation, and ring closure to yield the NCA was conducted by  $\text{COCl}_2$  (similar to [78]). Scheme 8 depicts the generic synthetic pathway to poly(L-DOPA) via ROP of an OH-protected NCA, with elements from both reported approaches [79–81].

Random co-polymers of different  $\alpha$ -amino acids can be produced by this route, and Deming and co-workers [21,82] have synthesised co-polypeptides of L-DOPA with L-lysine [82] using the corresponding carboxybenzyl-protected NCA monomers. Aqueous solutions of co-polypeptides were treated with several oxidants, and the resulting gels were assessed for their adhesive strength by lap shear testing on different substrates. A L-lysine/L-DOPA 80/20 co-polymer showed good adhesive strength values ( $>2.0$  MPa) on aluminium, steel and glass substrates which were significantly higher (approximately 7-fold increase) compared to a poly(L-lysine) homopolymer control. However, adhesion on plastic substrates (PMMA, polyethylene, polystyrene) was poor (less than 0.5 MPa). A co-polymer with L-glutamic acid (namely L-glutamic acid/L-DOPA 95/5) was also reported [21], which showed a 9-fold increase in lap shear strength on aluminium compared to a poly(L-glutamate) homopolymer control. These early efforts demonstrated the importance of the L-DOPA presence with respect to interfacial adhesion.



**Scheme 8.** Synthesis of poly(L-DOPA) from ring-opening polymerisation (ROP) of L-DOPA N-carboxyanhydride (NCA), Arrows in steps 1–2 refer to the two reported routes ([79,80], **bottom**; [81], **top**) with the acetylated derivative from [81] shown here. Reaction scheme adapted from [81], with permission. Copyright (2004) John Wiley and Sons.

In a related effort to produce direct mimics of MFPs, Statz and Messersmith et al. produced a range of L-DOPA-functionalised peptoids [83–85]. The latter are synthetic polypeptide analogues based on N-substituted glycine as the repeat unit. Standard solid phase peptide synthesis techniques were used to produce poly(N-substituted glycine) variants with different pendant groups (e.g., N-methoxyethyl, N-hydroxyethyl, N-hydroxypropyl) and a small number of L-DOPA and other residues to mimic the MFP structure and enhance adhesion. The peptoid part of the molecule was claimed to impart good antifouling properties against protein adsorption and cell attachment, with the L-DOPA moieties ensuring good adhesion on TiO<sub>2</sub> surfaces which were primarily tested as substrates. Scheme 9 shows a reported peptoid/peptide polymer.

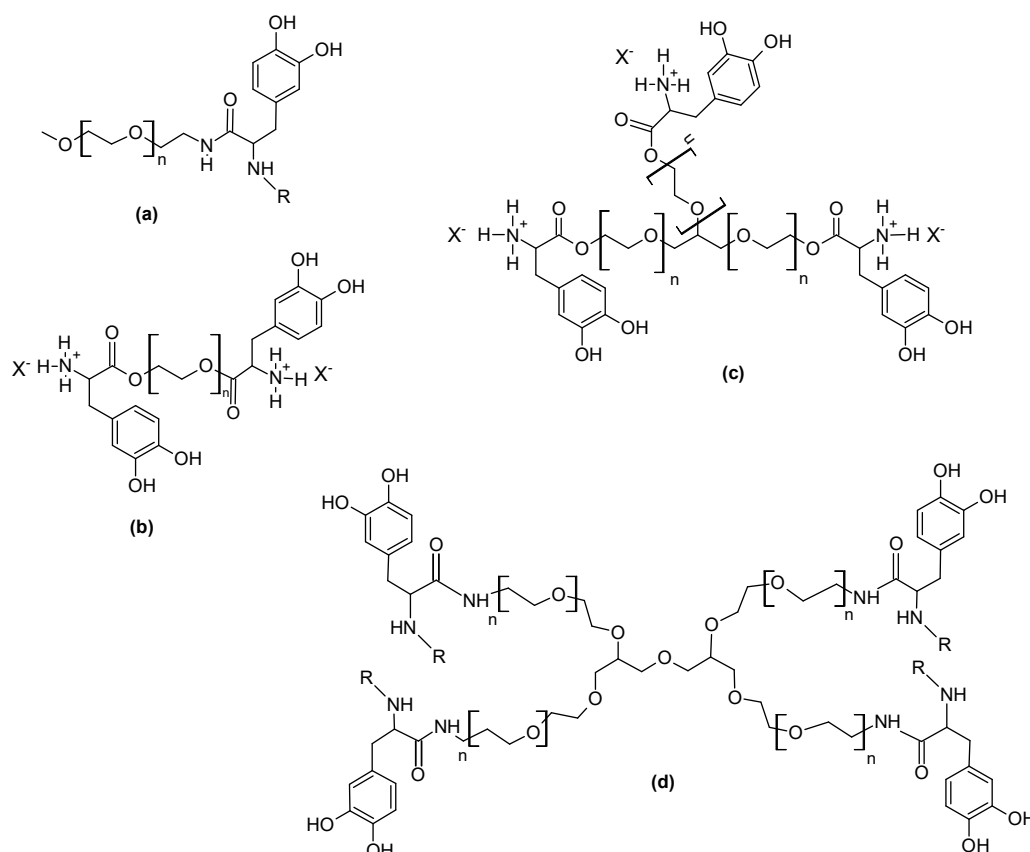


**Scheme 9.** Structure of a N-methoxyethyl-substituted peptoid with three additional L-DOPA residues for MFP adhesion mimicking [83]. Re-drawn from [83], with permission. Copyright (2005) American Chemical Society.

The resemblance of the N-methoxyethyl side chain in the peptoids discussed above to the repeat unit of poly(ethylene glycol)s, PEGs, has been amongst the reasons for selecting it [83]. PEGs are eminent hydrophilic polymers used in a variety of fields (including biocidal-free antifouling coatings—see Introduction) and with a very good account of antifouling performance, particularly against non-specific protein adsorption [86]. Similar to other hydrophilic polymers (e.g., zwitterionic polymers, polysaccharides), the antifouling mechanism is believed to be related to the presence of a

layer of water molecules strongly bound to the adsorbed hydrophilic polymer (known as hydration layer or shell) [87,88]. For fouling species (e.g., a protein molecule) to approach and attach onto the substrate, water molecules would need to be removed from the hydration layer. As for hydrophilic polymers the affinity between polymer and water is increased and the hydration layer strongly bound to the adsorbed polymer, this water molecule removal would be energetically very costly and unfavourable for the overall system [87,88]. Specifically for PEGs [86], they show some of the highest water solubility values amongst synthetic polymers, and furthermore maintain an extended conformation in water, which in turn results to high chain mobility for the PEG adsorbate, and an associated increased excluded volume (again preventing the approach and attachment of fouling molecules).

PEGs have been extensively utilised by the Messersmith group and others, and a range of catechol/L-DOPA modified PEGs have been reported [61,64,75,89–94]. PEGs are highly versatile polymers in terms of available molecular weight ranges (from ethylene glycol and oligomers of a few repeat units to  $10^6$  Da molecular weights for poly(ethylene oxide), PEO, materials), morphology (linear, branched, star, dendritic and hyperbranched), functionality (mono- and bifunctional, tri- and tetra-functional, polyfunctional) and end-group chemistry (traditional hydroxyl-terminated; other terminal functionalities such as methoxy, amine, thiol, acrylate, carboxy; homofunctional or heterofunctional) and hence provide a platform of options in order to produce a plethora of catechol-decorated variants. Some of the most characteristic structures are detailed below and depicted in Scheme 10.



**Scheme 10.** Mussel-inspired PEG structures: (a) monofunctional [90], (b) bifunctional [75], (c) trifunctional [75], (d) tetrafunctional [90].  $X^-$ :  $\text{TosO}^-$ , R: H- or Boc. Structures a, d re-drawn from [90], with permission. Copyright (2002) American Chemical Society. Structures b, c re-drawn from [75], with permission. Copyright (2019) John Wiley and Sons.

The first reports of L-DOPA-functionalised PEG or PEO materials were from the Messersmith group [89,90]. Succinimide-based end-group modification of hydroxyl-terminated commercially available PEO block copolymers with poly(propylene oxide), PPO (Pluronic F127 and F68, used as non-ionic surfactants) was followed by reaction with either L-DOPA or its methyl ester, yielding catechol-modified PEO-PPO with carboxy or methyl ester functionalities, respectively [89]. The effect of the L-DOPA modification on solution self-assembly and gelation was investigated by means of rheology and differential scanning calorimetry (DSC). Lee and Messersmith et al. produced some of the most recognizable and highly cited PEG-DOPA variants [90], including a methoxy-terminated monofunctional linear PEG-DOPA and a tetrafunctional 4-arm star structure (Scheme 10a,d), using a carbodiimide coupling approach between amine-terminated PEGs and the carboxylic acid group of the *t*-butyloxycarbonyl (Boc) protected L-DOPA. The Boc group can be subsequently removed, or not. These 4-arm catechol-functionalised PEGs in their different variants have been used extensively to make hydrogels by oxidative cross-linking (PEG-*N*-Boc-DOPA from [90] in [64]; a similar structure from the reaction of a pentaerythritol-derived 4-arm PEG-NH<sub>2</sub> with 3,4-dihydroxyhydrocinnamic acid [91]) and study their properties for a variety of (mainly medical) applications [91,92].

A linear methoxy-terminated succinimidyl propionate functionalised PEG (mPEG-SPA) was reacted directly with L-DOPA (similar to [89]) to produce a mono- to tri- functional methoxy-terminated PEG-DOPA [61]. This molecule was used as a coating on TiO<sub>2</sub> against protein adsorption, and the mechanism of catechol adhesion to the TiO<sub>2</sub> substrate and presence of mPEG-DOPA coating on the surface were studied with X-ray photoelectron spectroscopy (XPS). Excellent resistance against human serum protein adsorption was claimed for the mPEG-DOPA coated TiO<sub>2</sub> surfaces.

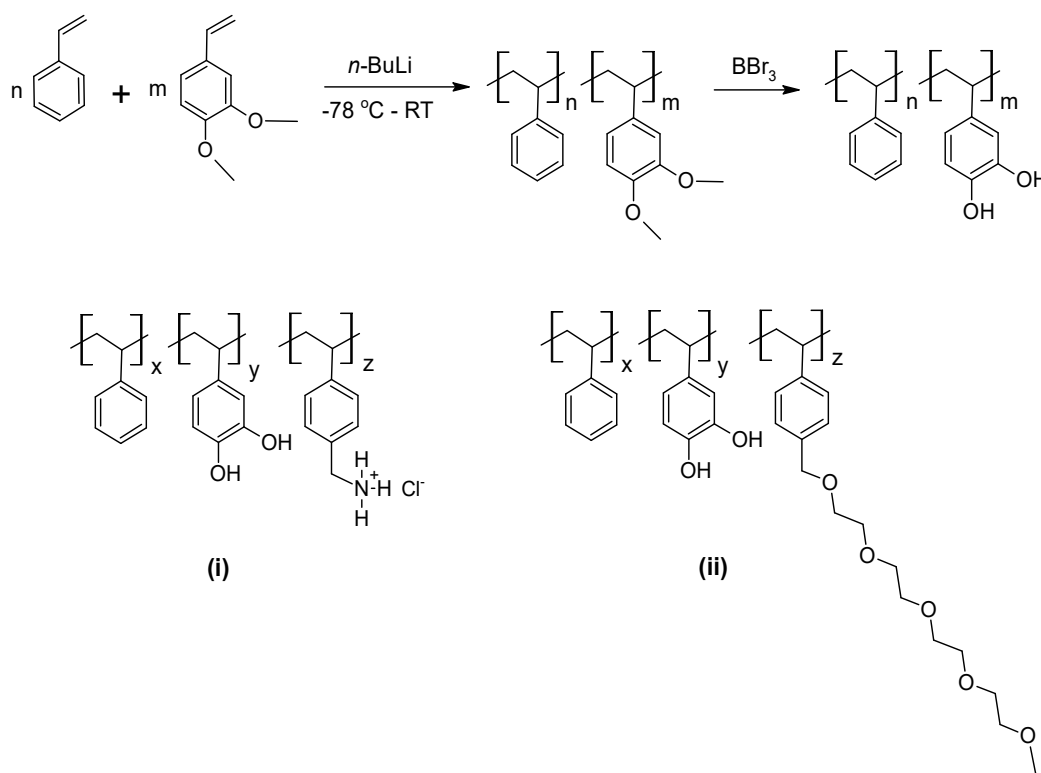
A number of further mussel-inspired PEG modification strategies and approaches have been reported [75,93,94], utilizing either chemistries on the hydroxyl end or pendant groups, or using PEGs modified with different functionalities and yielding various polymer morphologies and their corresponding coatings and gels. For example, Lee et al. [93] used *p*-nitrophenyl chloroformate to react with a pendant *sec*-OH group in their PEG backbone to produce a *p*-nitrophenyl ester and then couple with dopamine to yield a catechol side-chain. In our related previous work [75], we synthesised a range of oligomeric PEG-DOPAs (linear and trifunctional) by direct condensation reaction with L-DOPA [75,95] and studied their adsorption on various substrates by contact angle and XPS measurements, confirming the presence of a PEGylated surface and suggesting the occurrence of intermolecular interactions between the catechol-bearing end-groups. As the diversity of accessible/commercially available PEG variants continues to grow, further relevant modification and coupling chemistries will continue to appear (e.g., click-type chemistry using PEG-N<sub>3</sub> [94]).

Lastly, a related class of aliphatic hydroxyl-terminated polyethers known as hyperbranched polyglycerols (HPGs) [96–101] has shown great promise as functional macromolecules [96,97], including use of their catechol-modified variants as antifouling coatings [98,100,101]. These well-defined, low-polydispersity hyperbranched polymers are synthesized by the so-called ring-opening multi-branching polymerisation (ROMBP), first reported by Müllhaupt and co-workers [96]. The reaction involves the use of glycidol as a latent AB<sub>2</sub>-type monomer, and a poly-alkoxide initiator from a suitable deprotonated polyol (e.g., 1,1,1-tris(hydroxymethyl)propane [96–100], pentaerythritol [101]). Catechol functionalisation of the hyperbranched polyglycerol scaffold was performed using an amine-decorated HPG and 3,4-dihydroxyhydrocinnamic acid (hydroxyl-protected [99], or not [98]), resulting in a high density of available catechol groups compared to linear counterparts. The approach taken in [101] will be discussed in detail in Section 4, as it involves antifouling testing against a marine diatom.

While mussel-inspired PEG derivatives and related structures focused mainly on end-group coupling chemistries and coating/hydrogel applications in the biomedical field, the quest for simple, high molecular weight synthetic analogues of MFPs which would resemble their adhesive properties continued—with both chain-growth [102–112] and step-growth [95,113–115] high polymers with catechol-bearing pendant chains being reported. The strategies followed were: (i) polymerisation of catechol-bearing monomers (with protected hydroxyl groups, or not, depending on the polymerisation

conditions); (ii) post-synthesis modification of high molecular weight polymers with suitable catechol-functionalised agents. The latter approach extended also to various biopolymers [116]. Most of the above efforts focused on the incorporation of the catechol moiety as the key feature, while some also attempted to introduce some of the other characteristics identified in the MFPs (e.g., the presence of cationic residues).

The Wilker group has worked extensively on the mussel-inspired modification of one of the most important industrial chain-growth polymer commodities: polystyrene [102–105]. Poly(styrene-*co*-3,4-dihydroxystyrene) was produced via anionic polymerisation of styrene and 3,4-dimethoxystyrene, followed by removal of the methoxy groups by  $\text{BBr}_3$  [102] (Scheme 11). The catechol pendant groups imparted adhesion to aluminium comparable to commercial cyanoacrylates as indicated by lap shear testing [103], with optimal adhesion observed for approximately 30% mole 3,4-dihydroxystyrene content. More elaborate synthetic approaches yielded terpolymer structures employing additional cationic side chains (with a benzyltriethylammonium chloride pendant moiety [104]) as a more detailed MFP mimic, or additional functional oligo(ethylene glycol)-based side chains (in an effort to bring together high DOPA-mediated adhesion and anti-adhesive/antifouling PEG properties [105]). The relevant terpolymer structures are shown in Scheme 11.



**Scheme 11.** Random poly(styrene-*co*-3,4-dihydroxystyrene) by anionic polymerisation [102], **top**; related terpolymers with (i) benzyltriethylammonium chloride pendant moiety [104] and (ii) anti-adhesive oligo(ethylene glycol) pendant chain [105]. Structures re-drawn/adapted from reference [102,104,105], respectively. Copyright (2007, 2011, 2012) American Chemical Society.

A very versatile chain-growth monomer that has been extensively utilised to produce various linear and hyperbranched chain-growth MFP mimics is dopamine methacrylamide. Lee et al. [67] synthesised their smart adhesive hydrogels using a free-radical polymerisation approach in water, combining dopamine methacrylamide with *N*-hydroxyethyl acrylamide and 3-acrylamido phenylboronic acid, with methylene bis-acrylamide as bifunctional cross-linker and 2,2-dimethoxy-2-phenylacetophenone as ultraviolet (UV) photoinitiator. Washburn and co-workers [106] followed a microwave-assisted solventless free-radical approach, combining dopamine methacrylamide with 2-methoxyethyl acrylate

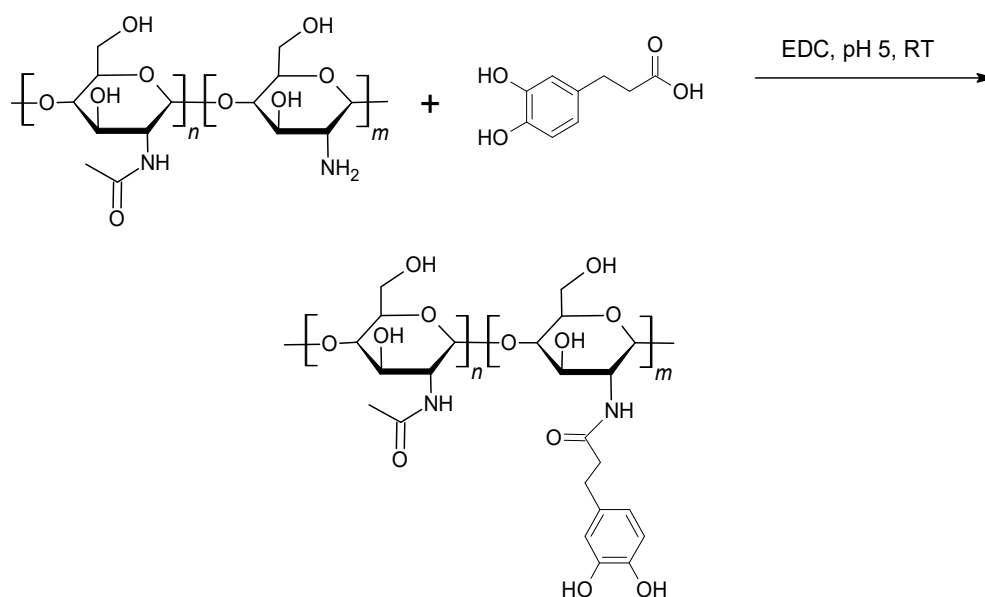
and ethylene glycol dimethacrylate as the bifunctional cross-linker, aiming to optimise the viscoelastic properties of the synthesised polymers for pressure-sensitive adhesive applications. With the overall research interest in hyperbranched polymers growing due to their high-density multifunctional backbone (see discussion on HPGs above [96–101]), so has the interest in catechol-functionalised hyperbranched chain-growth polymers by the traditional free-radical and most recently controlled radical polymerisation approaches (and specifically reverse addition-fragmentation chain transfer polymerisation, RAFT) [107]. Wang and co-workers reported hyperbranched PEG-DOPA polymers by RAFT [108,109], combining dopamine methacrylamide with methylether acrylate and diacrylate species of various oligo(ethylene glycol)s, targeting biomedical applications such as tissue adhesives [108] and anti-fibrillation agents in Parkinson's [109]. Lastly, post-synthesis modification of chain-growth polymers with catechol-bearing agents has also been explored, including poly(acrylic acid) [110] and poly(*N*-vinyl-2-pyrrolidone) copolymers with crotonic acid [111] being modified with dopamine, and maleic anhydride copolymers modified with L-DOPA [112].

Furthermore, polymers from step-growth polymerisation of L-DOPA/catechol functionalised building blocks (with protected or unprotected catecholic hydroxyls) have been reported [95,113,114], including poly(ester amide)s [95], poly(ester urea)s [113], solution-polymerised polyesters with hydrophobic pendant groups [114] using an acetonide-protected catechol-bearing diol co-monomer, and bulk-polymerised dopamine-end-capped polyesters [115], where linear oligo(ethylene glycol)s ( $M_n$  ranging between 400–1000 Da) were reacted with citric acid at 140–160 °C under vacuum to yield a pre-polymer, which was then crosslinked with sodium periodate and tested for surgical adhesive applications. In our previous work [95], we synthesised a range of novel L-DOPA-bearing monomers from various diols and polyols (by directly reacting unprotected L-DOPA in an esterification reaction), which were reacted further as bifunctional amine monomers with bis-(4-nitro-phenyl) sebacate to yield linear poly(ester amide)s, with promising results as bio-based pressure-sensitive adhesives.

Post-synthesis mussel-inspired chemical modification of high polymers, either in the form of end-group chemistries (see paragraphs on PEGs [61,64,75,89–94,96–101]) or via reactions to create catechol-bearing pendant groups (see paragraphs on chain-growth polymers [110–112] and step-growth polymer end-capping [115]), has been a very popular and successful approach to impart mussel-like adhesion or self-healing to known polymers with useful properties. Apart from the examples presented previously, mussel-inspired derivatives of various biopolymers [116] have attracted attention for their potential as multifunctional materials. Amongst the various catechol-derivatised biopolymers, polysaccharides (e.g., alginate [117,118], chitosan [119–123], hyaluronic acid [124], fucoidan [125], heparin [126,127]) hold a prominent position due to their set of attractive properties (e.g., biocompatibility, antimicrobial action, drug delivery). Coupling chemistries have either used dopamine reacting with available carboxyl groups [117,118,124–127], or 3,4-dihydroxyhydrocinnamic acid reacting with available amine groups [119–123] such as in the case of chitosan (Scheme 12).

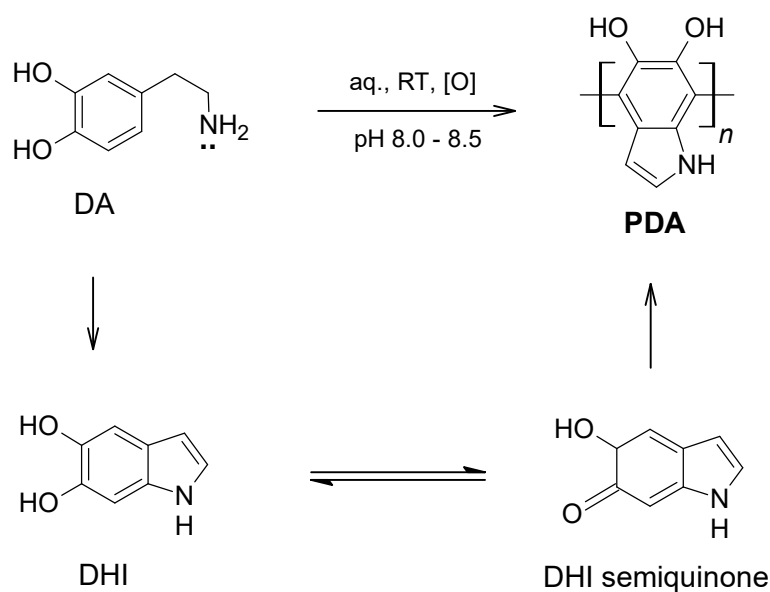
Perhaps the most famous mussel-mimetic synthetic polymer material, and coating in particular, is poly(dopamine), PDA [44,65,128–135], stemming from the oxidative polymerisation of dopamine in aqueous alkaline solutions. Virtually any substrate dip-coated in such a solution will receive a spontaneously formed adsorbate layer from the oxidation-driven self-polymerisation of dopamine, while self-assembled dopamine aggregates will form at the same time in solution. In the original report by Lee and Messersmith [65], the aqueous buffer solution used was a 10 mM tris(hydroxymethyl)aminomethane hydrochloride (Tris HCl, pH 8.5) at ambient conditions (air, room temperature) and with no additional oxidant other than dissolved atmospheric oxygen. An insoluble, dark-coloured coating was observed on objects immersed in this solution within a few hours. The coating development was monitored over time, with higher thicknesses achieved for longer immersion times, reaching 50 nm in 24 h. XPS confirmed the presence of a coating on the substrate and revealed a nitrogen-to-carbon signal ratio of 0.10–0.13, consistent with the 0.125 value for dopamine (suggesting that the formed coating is the result of the polymerisation of the dissolved dopamine). Most interestingly,

this coating develops in a substrate-agnostic way: similar features (thickness development, XPS analysis) were invariably observed on metal, ceramic or plastic substrates.



**Scheme 12.** Modification of chitosan with 3,4-dihydroxyhydrocinnamic (hydrocaffeic) acid in the presence of 1-ethyl-3-(3-dimethylaminopropyl)-carbodiimide (EDC) hydrochloride, yielding catechol-functionalised chitosan [123].

While the characteristics of polydopamine and its in-situ formed coatings appear remarkably universal, the precise structure of the polymer remains a subject of debate [44,129–132]. There is currently consensus that the polymerisation is oxidative and is promoted by the alkaline pH in the original report [65] via a pathway that includes quinone formation (Scheme 3), followed by inter-molecular ring-closure reaction of the amine group to form an indole structure (5,6-dihydroxyindole, DHI; Scheme 13)—amongst other possible covalent structures. A combination of covalent and non-covalent interactions (mainly  $\pi$ - $\pi$  stacking) has been claimed to occur and effectively impart the observed lack of solubility of the polydopamine coating [44,128–131]. However, even with the exact structure elusive and subject to an ongoing debate, post-functionalisation of the formed polydopamine coating in line with the discussed catechol covalent reactions with nucleophiles (Scheme 4) has been conveniently applied in the first report [65] and extensively thereafter. Specifically in the original PDA study [65], polydopamine-coated surfaces were exposed to solutions of linear aliphatic thiols, thiol-functionalised oligo(ethylene glycol)s and thiolated hyaluronic acid (HA); yielding hydrophobic *pseudo* self-assembled monolayer, hydrophilic *pseudo* self-assembled oligoPEG monolayer and a HA-modified derivative, respectively. In all cases, the polydopamine modification was via Michael-type addition of thiol onto the catechol ring (Scheme 4d–f) and the new adlayer was verified by means of contact angle, XPS and other analyses (e.g., increased resistance to fibroblast cell attachment was observed for the oligoPEG-modified polydopamine coating). Lastly, the formation of metal Ag and Cu adlayers was reported, by exposing polydopamine-coated surfaces to  $\text{AgNO}_3$  and  $\text{CuCl}_2$  solutions, respectively, exploiting the discussed metal-binding affinity of catechols (Scheme 2).



**Scheme 13.** Generic scheme for polydopamine (PDA) formation via a reactive 5,6-dihydroxyindole (DHI) intermediate.

An array of studies (expanding in a very wide range of possible applications) summarised in several reviews [128–131] has followed the first polydopamine account [65], in which the process parameters were varied, aiming to address some of the issues with polydopamine coatings [128,129,131]: slow coating thickness build-up and high roughness (at least for some applications), narrow pH range, incorporation of Tris HCl in the polydopamine structure (due to its amine group) and at best modest mechanical properties. For this purpose, essentially all process parameters (concentration, solvent, temperature, immersion time, amine-free buffer molecules, additional oxidant, pH, additional UV/microwave energy) have been re-visited [128–131], including dopamine itself: it has been shown rather quickly that this oxidative self-polymerisation approach is applicable to a range of catecholamines, including L-DOPA itself [132] (this polymer however, poly(DOPA), is not to be confused with linear poly(L-DOPA) presented in Scheme 8), and norepinephrine [133]. Thermal annealing of PDA coatings (at 130 °C under vacuum) has been recently proposed as a facile way to enhance their mechanical robustness [134]. Even in the absence of amine groups in the monomer, simple catechol moieties (e.g., 4-heptadecylcatechol) can polymerise in the presence of aqueous ammonia (acting as the nucleophile) [135].

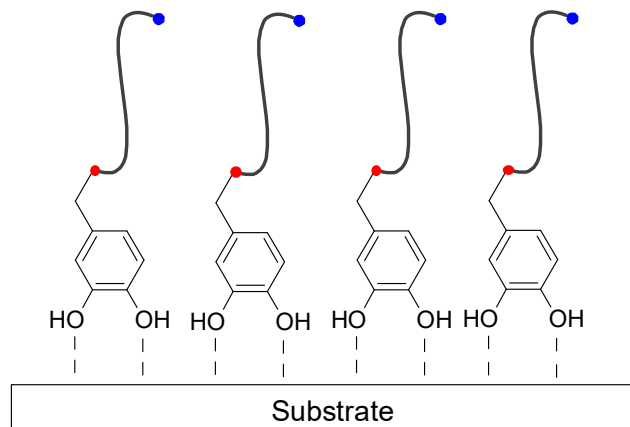
To summarise, the discovery of MFPs and their structure in the 1980s has led to a vibrant research field of synthetic MFP mimics, adopting one (or more) of the following approaches and strategies to yield a catechol-functionalised synthetic oligomer or polymer (a very comprehensive review of reported structures is given in [116]):

- Reaction of catechol-bearing monomers (with protected hydroxyl groups, or not) by step-growth, chain-growth (free radical or controlled radical polymerisation methods) and ring-opening pathways to catechol-bearing homo- and co-polymers.
- Modification of an existing polymer or oligomer with a catechol-bearing reagent; either end-capping, or coupling with main-chain functional groups to yield pendant catechol chains.
- Solid-phase supported peptide synthesis.
- Oxidative self-polymerisation of catecholamines: polydopamine and related materials.

Selected recent advances from systems falling into several of the above categories and specially designed/tested for marine antifouling will be presented in Section 4.

#### 4. Recent Advances in Mussel-Inspired Polymers as Marine Antifouling Coatings

A principle schematic of a catechol-anchored polymer or oligomer coating with antifouling properties is given in Scheme 14.



**Scheme 14.** Principle schematic of a mussel-inspired catechol-anchored antifouling coating. Red dots denote the chemical bond between catechol moiety and antifouling polymer/oligomer (depicted by a generic chain with a functional chain-end for antifouling capacity—blue dot). Dashed lines refer to the bond of catechol moiety to the surface of the substrate, this being covalent (Schemes 4 and 6) or non-covalent (Scheme 7).

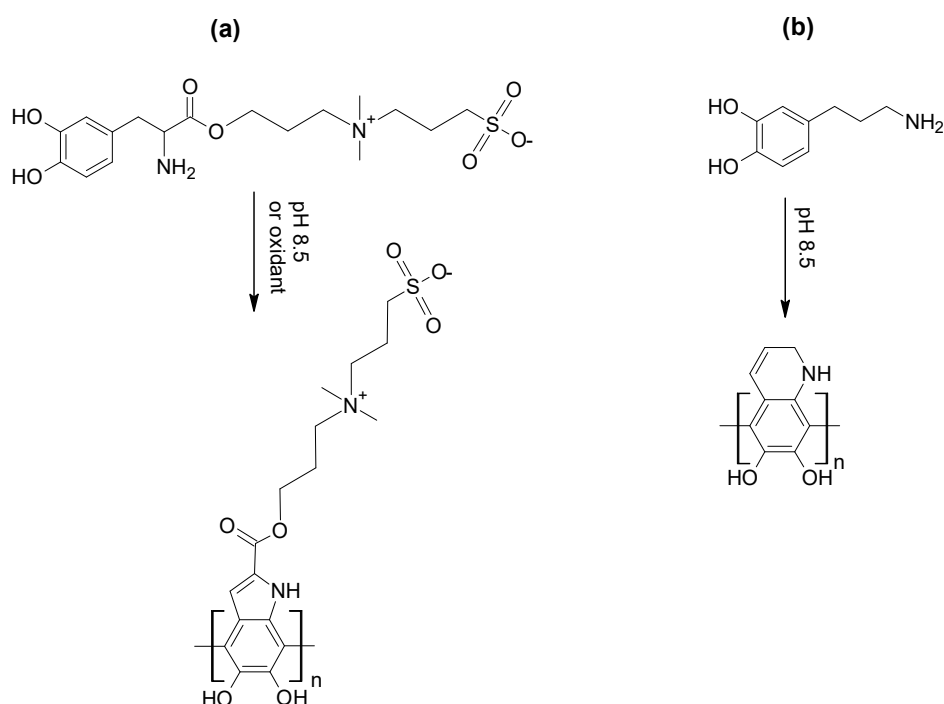
The generic catechol-derivatised antifouling polymer/oligomer structure may refer to any of the synthetic MFP mimics discussed in Section 3.2.4, and depending on its length it may be referred to as self-assembled monolayer (e.g., [62]), *pseudo* self-assembled monolayer from the functionalisation of a polydopamine primer [65], polymer brush (for oligomers) or coating (for high polymers). Attachment to the substrate may be facilitated by the different covalent and non-covalent routes discussed in Sections 3.2.1–3.2.3. In this section, we review some of the most recent studies which report a mussel-inspired oligomer/polymer derivative and coating, designed and/or tested for resistance against marine biofouling species.

##### 4.1. Polydopamine-Type Materials

Two novel catecholamine derivatives [136,137] have been recently reported as options for surface-independent oxidative poly(catecholamine) coatings, specifically for marine antifouling.

The first catecholamine is a zwitterionic molecule: 3-((3-((2-amino-3-(3,4-dihydroxyphenyl)propanoyl)oxy)propyl)dimethylammonio)propane-1-sulfonate, ZW-DOPA [136]. The second catecholamine is a simple dopamine derivative with one additional methylene group: 4-(3-aminopropyl)-benzene-1,2-diol, or 3-catecholpropanamine, CPA [137]. Both structures and their oxidative polymerisation products are depicted in Scheme 15.

ZW-DOPA was synthesised from L-DOPA in a six-step synthetic protocol (including several column chromatography purification steps for intermediates and final product). Zwitterionic polymers have been identified as strong candidates for antifouling purposes due to their structural similarity to the phosphatidylcholine-based phospholipid bilayers of cell membranes [87,88,138], and are generally classified as polybetaines (when positive and negative charge are present on the same monomeric unit or side chain) and polyampholytes (when positive and negative charges are present on separate monomeric units or side chains) [138]. In this respect, ZW-DOPA and its oxidative polymerisation product are part of the betaine family (Scheme 15).



**Scheme 15.** Structures for (a) ZW-DOPA and poly(ZW-DOPA) [136] and (b) CPA and poly(CPA) [137]. Structures re-drawn/adapted from reference [136] (a) and reference [137] (b), with permission. Copyright (2018, 2019) American Chemical Society.

Coatings of poly(ZW-DOPA) were deposited on stainless steel and Ti/TiO<sub>2</sub> (metal Ti with native TiO<sub>2</sub> layer) substrates. The polymerisation and coating process involved the use of a 2 mg/mL ZW-DOPA solution in a Tris HCl buffer (pH 8.5), as well as the use of additional oxidants (ammonium persulfate and sodium periodate; when additional oxidants were used, ZW-DOPA was dissolved in water at 2 mg/mL, in a 2:1 molar ratio to the oxidant). The coating time was kept at 24 h, and the coating thickness on Ti/TiO<sub>2</sub> increased from the alkaline pH/no oxidant condition, to ammonium persulfate and sodium periodate (reaching almost 40 nm for the latter). The effect on static water contact angle values followed the same trend (from 47° for the bare substrate, to ~38° for the alkaline pH condition/tris HCl buffer only, to ~12° for the ammonium persulfate and less than 10° for the sodium periodate treatment), indicating a much more hydrophilic surface for the oxidant-coated poly(ZW-DOPA) samples. Similar trends were observed for stainless steel and Nylon substrates (for the sodium periodate treatment versus the uncoated reference).

Antifouling testing against the marine diatom *Amphora coffeaeformis* was conducted on stainless steel and Ti/TiO<sub>2</sub> substrates coated with poly(ZW-DOPA), with all three sets of coating conditions/treatments, and with striking effects. Coated samples were immersed in a diatom cell suspension for 24 h, and attached diatom density was assessed by fluorescence imaging. The observed density of adhered diatoms was reduced from 165 diatoms per image for the bare Ti/TiO<sub>2</sub> to 125, 66, and 10 diatoms per image for Tris HCl buffer (no oxidant), ammonium persulfate and sodium periodate treatment, respectively. Similar antifouling behavior enhancement was observed for stainless steel (288 diatoms per image for uncoated versus 3 diatoms per image for sodium periodate treated poly(ZW-DOPA)) and Nylon (42% reduction from bare to sodium periodate poly(ZW-DOPA)).

A basic antifouling durability test was also conducted for the stainless steel samples, and the diatom assay was performed on bare and sodium periodate treated poly(ZW-DOPA)-coated stainless steel after immersion in seawater for 28 days. Diatom adhesion density for the sodium periodate/poly(ZW-DOPA) coated sample was still 52% lower than that of the uncoated reference.

In the study [137] of 4-(3-aminopropyl)benzene-1,2-diol (or 3-catecholpropanamine, CPA), the target molecule was synthesised from 3,4-dimethoxybenzaldehyde in seven steps. Coatings of

poly(CPA) were deposited on Ti/TiO<sub>2</sub> (as in [136]) and a range of other substrates (e.g., stainless steel, glass, gold, Nylon, PTFE), using a 2 mg/mL CPA solution in a Tris HCl buffer (pH 8.5) with no additional oxidant. The coating time was varied up to 24 h, and the obtained poly(CPA) coating thickness was compared to that of polydopamine deposited under the same conditions. All poly(CPA) coated substrates showed static water contact angle values around 33° and were different from the corresponding bare substrate, while the poly(CPA) coatings appeared to reach higher thickness values and at a higher rate compared to polydopamine.

Furthermore, the poly(CPA) coatings obtained were modified with an amine-terminated PEG (PEG-NH<sub>2</sub>) via nucleophilic reaction with the amine group (Scheme 4) to study the antifouling performance of the resulting PEG-grafted poly(CPA). Interestingly, CPA was also used to modify fucoidan in an analogous manner as with dopamine [125]. A fucoidan-CPA coating was cast on Ti/TiO<sub>2</sub> after immersing in a 5 mg/mL solution in Tris HCl for varying times, and was studied for anti-platelet (from a human blood platelet solution) performance. More details on this are given in Section 4.3.

Antifouling testing against the marine diatom *Amphora coffeaeformis* was conducted again in this study, using Ti/TiO<sub>2</sub> substrates as follows: (i) untreated, bare substrate, (ii) poly(CPA)-coated, and (iii) PEG-grafted poly(CPA) surface. Coated samples were as before immersed in a diatom cell suspension for 24 h, and attached diatom density was assessed by fluorescence imaging. Diatom adhesion density was modestly reduced from 125 diatoms per image for the bare substrate to 100 for the poly(CPA)-coated sample. However, the diatom population diminished to only 10 diatoms per image (92% reduction) for PEG-grafted poly(CPA), demonstrating the effect of the grafted PEG chains. As the diatom antifouling testing conditions between these two studies are directly analogous, Table 2 presents a comparative evaluation of the efficacy of the different treatments discussed in [136,137] against *Amphora coffeaeformis*.

**Table 2.** Antifouling performance of poly(ZW-DOPA) and poly(CPA) coatings on Ti/TiO<sub>2</sub> against *Amphora coffeaeformis* [136,137] <sup>1</sup>.

Sample	Diatom Adhesion Density (Diatoms per Image)	% Reduction <sup>2</sup>	Ref.
Bare Ti/TiO <sub>2</sub>	165	-	[136]
Poly(ZW-DOPA) coated <sup>3</sup>	125	24	[136]
Poly(ZW-DOPA)/ammonium persulfate	66	60	[136]
Poly(ZW-DOPA)/sodium periodate	10	94	[136]
Bare Ti/TiO <sub>2</sub>	125	-	[137]
Poly(CPA) coated <sup>3</sup>	100	20	[137]
PEG-grafted poly(CPA)	10	92	[137]

<sup>1</sup> 24 h exposure to diatom suspension at ambient conditions. <sup>2</sup> Relative to related bare substrate. <sup>3</sup> In Tris HCl (pH 8.5).

#### 4.2. Poly(Ethylene Glycol) (PEG) Based Materials

*Amphora coffeaeformis* has been a frequently used model for marine antifouling assays, and this has been the case with two further studies [101,139] incorporating a PEG-based material in their proposed coating. Kang and co-workers [139] produced a multilayered coating (Figure 4) on various substrates (e.g., stainless steel, Nylon, Ti/TiO<sub>2</sub>, SiO<sub>2</sub>) using a polydopamine primer on which a 6-arm PEG-DOPA was spin-coated. The resulting coated sample was immersed in a FeCl<sub>3</sub> solution followed by incubation at pH 7.4, aiming to establish Fe<sup>3+</sup>—catechol reversible cross-links in the multilayered construct (within or between layers) and thus enhance its mechanical robustness.

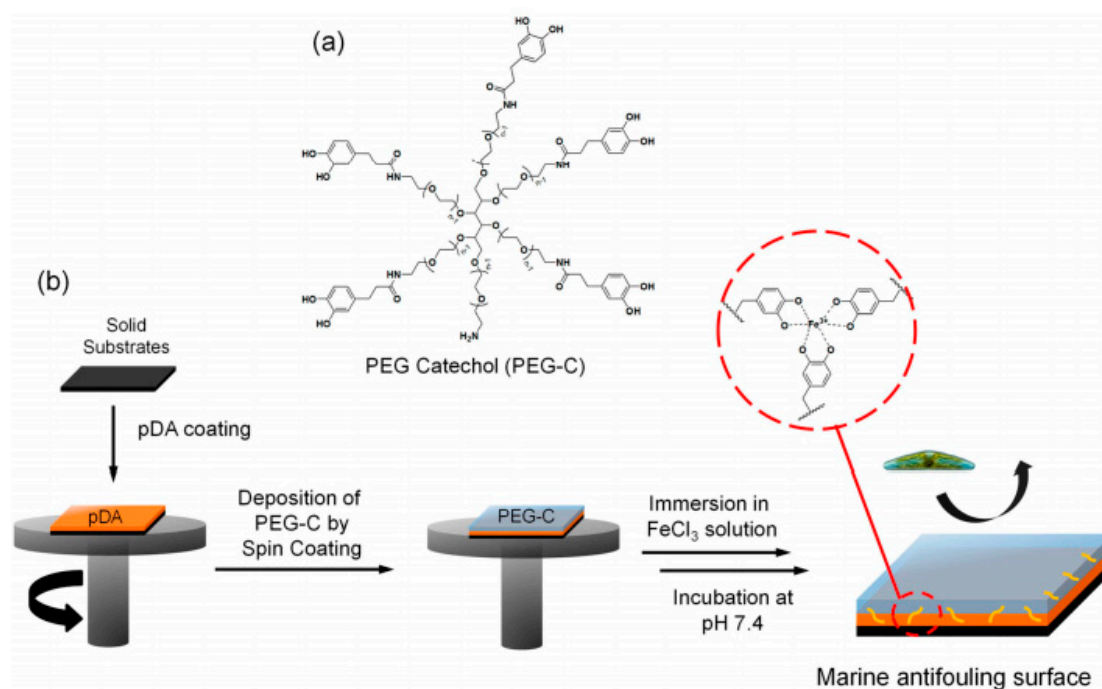


**Figure 4.** (a) Structure of 6-arm PEG-DOPA synthesised and used by Kang et al. [139]; (b) Schematic representation of the approach followed by Kang et al. to produce a PDA/PEG-DOPA/Fe<sup>3+</sup> multilayer coating. Reproduced with permission from reference [139]. Copyright (2018) American Chemical Society.

As in the studies discussed in Section 4.1, antifouling testing against the marine diatom *Amphora coffeaeformis* was again conducted on stainless steel substrates coated with (i) PDA primer only, and (ii) the complete PDA/PEG-DOPA/Fe<sup>3+</sup> multilayer. Coated samples were (as in [136,137]) immersed in a diatom cell suspension for 24 h, and attached diatom density was evaluated by fluorescence imaging. Diatom density dropped from 183 diatoms per image for the bare substrate to 145 for the PDA primer coated sample, and to 20 for the PDA/PEG-DOPA/Fe<sup>3+</sup> (87% reduction relative to the bare substrate), thus exhibiting very similar trends to those noted in Table 2. A PDA/PEG-DOPA/Fe<sup>3+</sup> coated Ti/TiO<sub>2</sub> substrate also showed a very significant decrease (7 to 8-fold) in attached diatom density compared to the bare substrate.

Furthermore, a durability test was performed on stainless steel samples (bare and coated by PDA/PEG-DOPA/Fe<sup>3+</sup>), by immersing in seawater for 1–4 weeks and followed by the *Amphora coffeaeformis* diatom assay. Even after 4 weeks in seawater, the PDA/PEG-DOPA/Fe<sup>3+</sup> showed a 50% lower diatom count compared to that of untreated stainless steel after 24 h exposure. The loss of antifouling capacity was attributed to the potential oxidation of PEG in the presence of Fe<sup>3+</sup>.

Teo and Kang and co-workers [101] synthesised HPGs by ring-opening multi-branching polymerization (ROMBP), using glycidol and pentaerythritol as the poly-alkoxide initiator. Rather than proceeding towards catechol-functionalised derivatives of their HPGs, they synthesised thiol-functionalised HPGs (HPG-SH) with different degrees of thiolation (ranging in -SH content from 0.8% to 26%). The thiol groups were subsequently used as coupling agents to attach the HPG block on a range of mussel-inspired primer coatings on stainless steel, namely: (i) monolayer of *N*-dopamine maleimide, (ii) tannic acid, and (iii) polydopamine. The thiol groups present on the periphery of the HPGs bind to these primers in either a thiol-ene reaction (for *N*-dopamine maleimide) or by Michael-type addition on the catechol moieties (Scheme 4d–f). Higher thiol content in HPGs resulted in higher grafting density and hence higher coverage of the primer, and in turn to higher thickness and lower roughness for the overall coating. The presence of disulfide bonds as a cross-linking pathway

was identified and correlated to the coating attributes and -SH content. Figure 5 depicts a schematic overview of the process.

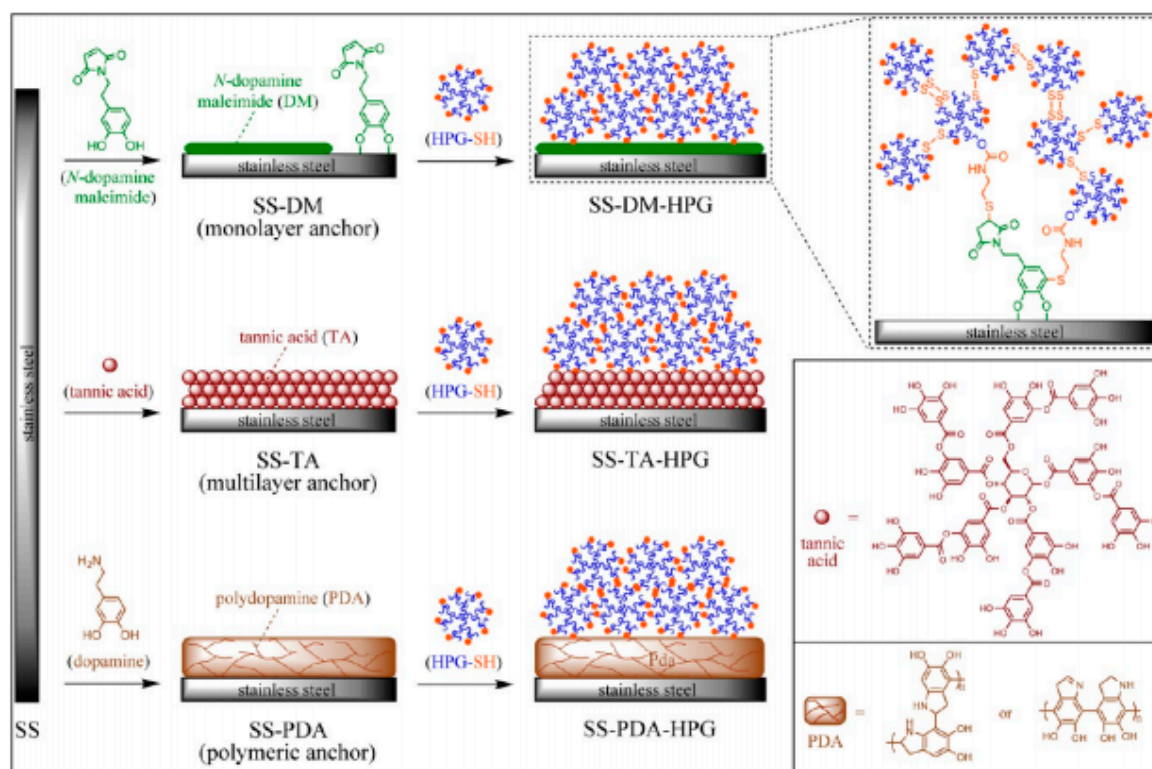


**Figure 5.** Schematic representation of the HPG-SH structure and the coating approach followed by Teo and Kang and co-workers [101] with covalent attachment of HPG-SH on three mussel-inspired primers on stainless steel (monolayer of *N*-dopamine maleimide, **top**; tannic acid, **middle**; polydopamine, **bottom**). Reproduced with permission from reference [101]. Copyright (2016) American Chemical Society.

In terms of marine antifouling assessment, *Amphora coffeaeformis* was once more selected as the model system. Surfaces were immersed in a  $10^5$  cells/mL diatom suspension for 24 h at ambient conditions, with the difference compared to the previous studies [136,137,139] that the quantification was performed by a peel-off step after sonication and fluorescence spectroscopy (rather than fluorescent image count). The fact itself that attached diatoms could be removed for quantification by a benign treatment (sonication in water for 10 min) was highlighted as evidence of the weak bond between foulers and coatings. On the pristine stainless steel substrate, a diatom count of 14,600 cells/cm<sup>2</sup> was reported, with primer-only coatings also showing elevated colonisation levels with 13,800, 13,100 and 13,300 cells/cm<sup>2</sup> measured for *N*-dopamine maleimide, tannic acid and polydopamine primer, respectively. In contrast, however, the HPG-modified multilayers showed a much improved performance against the diatom attachment, which increased with the -SH group (and grafting) density: with 5200 diatom cells/cm<sup>2</sup> for the PDA-primer HPG with thiol content of 0.8%, to 1500 diatom cells/cm<sup>2</sup> for the PDA-primer HPG with thiol content of 26%. Similar trends were recorded for the 26% thiol content HPGs on tannic acid and *N*-dopamine maleimide primers, with 3330 and 2600 diatom cells/cm<sup>2</sup>, respectively.

Lastly, Hawker and collaborators [140] reported in 2016 a very interesting MFP-2-mimicking PEG structure, which comprised a linear PEO triblock copolymer -namely poly(ethylene oxide-*co*-allyl glycidyl ether)-*b*-poly(ethylene oxide)-*b*-poly(ethylene oxide-*co*-allyl glycidyl ether)- with two functional side chains stemming from the allyl glycidyl ether segments and bearing a triethylsilyl-protected terminal catechol. The catechol groups were deprotected in situ under acidic

conditions during measurements and experiments. The loop-like conformation of polymers adsorbed on mica was claimed from data obtained by surface force apparatus (SFA) and near edge X-ray absorption fine structures (NEXAFS) measurements. Antifouling testing was performed against the red alga *Porphyra suborbiculata* using glass substrates coated with the catechol-functionalised PEO triblock copolymer. The coated samples exhibited significant reduction (more than 50%) compared to the bare glass in spore settlement at  $t = 1$  day after seeding.

#### 4.3. Polysaccharide and Polypeptide Materials

Two examples of catechol-derivatised polysaccharides (namely heparin [127] and fucoidan [125,137]) and one example of a catechol-functionalised antimicrobial peptide (Magainin II [141]) are presented here. Apart from their natural origin, the three biopolymers and the corresponding studies are linked in the context of this review as they follow the same catechol derivatisation approach. Dopamine is used as the catechol-bearing reagent in the presence of 1-ethyl-3-(3-dimethylaminopropyl)-carbodiimide (EDC) hydrochloride (see Scheme 12), and an amide bond is created from the reaction with available carboxyl groups in the three macromolecules (glucuronic acid residues in fucoidan, iduronic acid residues in heparin and two carboxylic acid groups in magainin II: one in the C-terminus from serine, and one from the side chain of the one glutamic acid present). Moreover, all three studies [125,127,141] focused to a large extent on stainless steel as substrate, due to its importance as structural material in marine vessels and structures.

Successful conjugation of dopamine and the presence of the catechol moiety in the modified heparin [127] backbone was confirmed and quantified by UV spectroscopy (presence of absorbance peak at 280 nm). Stainless steel coupons were immersed in a 5 mg/mL solution of dopamine-modified heparin in a 10 mM Tris HCl solution (pH 8.5) for 24 h. The heparin-catechol coated substrates were tested for their antifouling potential against two marine diatom species: *Navicula perminuta* and *Amphora coffeaeformis*, after a 4 h exposure to a cell suspension at room temperature and quantification by fluorescence imaging. The mussel-inspired heparin coatings exhibited reduced diatom attachment density against *Amphora coffeaeformis* by 73% compared to uncoated stainless steel, and against *Navicula perminuta* by 75% compared to the bare substrate.

In the case of the fucoidan-dopamine derivative reported in [125], successful conjugation of dopamine and presence of the catechol moiety in the modified fucoidan backbone was again confirmed and quantified by UV spectroscopy (presence of absorbance peak at 280 nm), as well as by nuclear magnetic resonance ( $^1\text{H-NMR}$ , presence of aromatic protons) and Fourier transform infrared (FTIR, amide bond absorption band) spectroscopies. To produce coated specimens, stainless steel coupons (1 cm  $\times$  1 cm) were immersed in a 5 mg/mL solution of fucoidan-dopamine in Tris HCl buffer (pH 8.5) for 24 h. A similar *Amphora coffeaeformis* assay was again conducted (4 h exposure to the diatom cell suspension at room temperature; quantification by fluorescence imaging). A reduction of 65% in diatom attachment density compared to the bare stainless steel substrate was recorded. Finally, a durability assessment of the fucoidan-dopamine coatings was performed. Coated samples were immersed in seawater for 1–3 weeks, followed by the diatom attachment assay. After 3 weeks in seawater, the fucoidan-dopamine coated specimen showed reduced diatom attachment by 56% compared to the uncoated reference.

As mentioned in Section 4.1, CPA was also used to modify fucoidan [137] in an analogous manner as with dopamine [125]. A fucoidan-CPA polymer was thus synthesised and characterised (similar to fucoidan-dopamine [125]), and it was compared to a fucoidan-dopamine reference polymer made in the same study. The fucoidan-CPA coating was cast on a Ti/TiO<sub>2</sub> substrate by immersing in a 5 mg/mL solution in Tris HCl for varying times, and was studied for anti-platelet (from a human blood platelet solution) performance. A two-fold increase in coating speed was claimed for fucoidan-CPA compared to fucoidan-dopamine [137]. Furthermore, the anti-platelet assessment involved incubation at 36.5 °C for 24 h and observation of adhered platelets by SEM. A remarkable inhibition of cell attachment was

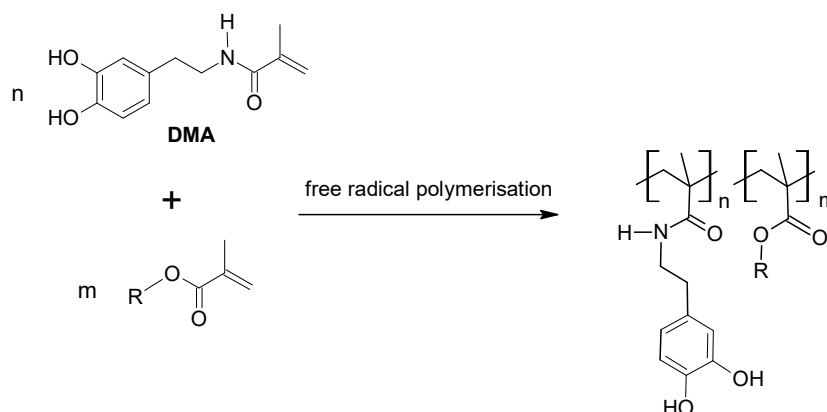
claimed at similarly very high levels for both fucoidan-CPA and fucoidan-dopamine, which should be attributed to the presence of fucoidan in both coatings.

Magainin II [141] is an antimicrobial peptide of animal origin (found in frog skin) and comprising a sequence of 23 aminoacids (Gly-Ile-Gly-Lys-Phe-Leu-His-Ser-Ala-Lys-Lys-Phe-Gly-Lys-Ala-Phe-Val-Gly-Glu-Ile-Met-Asn-Ser), with terminal glycine (N-terminus) and serine (C-terminus) residues. It also contains a glutamic acid (Glu) residue and thus has two carboxylic acid groups available for reaction with dopamine following the EDC chemistry described before [117,118,123–126], and synthesis of the dopamine derivative of magainin II. Stainless steel coupons (10 mm × 10 mm × 1 mm) were immersed in a solution of dopamine-magainin II in Tris HCl (pH 8.5) for 12 h, and the resulting coating was characterised by means of XPS (showing the suppression of Fe-related signals and the presence of new sulfur and nitrogen signals), contact angle (from 70.5° for bare stainless steel to 39° for the sample coated with the dopamine-magainin II conjugate) and atomic force microscopy, AFM (a rougher surface observed for the dopamine-magainin II coating compared to the smooth/polished pristine stainless steel). Antibacterial assays against two marine bacteria (*Vibrio natriegens* and *Citrobacter farmeri*) were conducted after incubation for 24 h and by means of SEM and fluorescent imaging (staining by propidium iodide). The dopamine-magainin II coated specimens were claimed to exhibit very low bacteria coverage (0.087% for *V. natriegens* and 0.070% for *C. farmeri*) compared to the uncoated references (40.6% for *V. natriegens* and 11.1% for *C. farmeri*). Lastly, a durability test was conducted after incubation with the same bacterial solutions for 1, 7, 14 and 21 days, where the dopamine-magainin II coatings showed good retention of their thickness and adhesion on the stainless steel substrate for different casting concentrations.

#### 4.4. Dopamine Methacrylamide Based Materials

As discussed in Section 3.2.4, one of the most versatile chain-growth monomers that has been utilised to synthesise various linear and hyperbranched chain-growth (co-)polymer structures [67,106–109] is dopamine methacrylamide, DMA (Scheme 16). Two relevant studies [142,143] have been recently reported. In the first study [142], dopamine methacrylamide was dissolved in dimethylformamide (DMF), together with a polydimethylsiloxane oligomer ( $M_n = 5.5$  kDa) bearing a mercaptopropyl (thiol) side chain, and an oligo(ethylene glycol) diacrylate as crosslinker. A UV photo-initiator (Igracure 651) was added and the mixture was cast on glass, steel or aluminum substrates and was UV-cured at 365 nm. Different coating compositions were prepared by varying the oligo(ethylene glycol) diacrylate and UV photo-initiator proportions (with a reference composition lacking any UV photo-initiator). Water swelling tests were conducted for the coated specimens, and the water uptake/degree of swelling was noted. All samples showed very low swelling (just above 3% after 7 days in distilled water). Protein adsorption was evaluated using lysosome and bovine serum albumin (BSA), by immersing the samples to a 50 µg/mL protein solution for 12 h. A significant reduction in adsorbed protein (qualitatively by fluorescence microscopy, and by a quantitative assay using bicinchoninic acid) was observed for all coating compositions against a polydimethylsiloxane-only control coating.

Marine antifouling was assessed against the *P. tricornutum* diatom. Glass slides coated with the different copolymers and a polydimethylsiloxane-only control coating were immersed in a diatom suspension for 7 days at 16 °C. Attached diatom density was evaluated by optical microscopy and a hemocytometer. All specimens performed better than the control ( $507 \times 10^3$  diatoms/cm<sup>2</sup>), with the copolymer composition of the highest oligo(ethylene glycol) diacrylate weight content and lowest photo-initiator weight content showing the best antifouling potential (less than  $100 \times 10^3$  diatoms/cm<sup>2</sup>; at least 5-fold reduction against the control) between the copolymers, with a clear trend established between composition (oligo(ethylene glycol) diacrylate and photo-initiator weight content) and *P. tricornutum* attachment.



**Scheme 16.** General reaction scheme for dopamine methacrylamide (DMA) free radical co-polymerisation with a generic methacrylate co-monomer.

In the second study [143], DMA was combined with 2,2,2-trifluoroethyl methacrylate (TFME) and  $\alpha,\alpha$ -azobisisobutyronitrile (AIBN) as initiator with DMF as solvent and under a nitrogen atmosphere—to minimise any oxidation side reactions of the catechol moiety in the presence of free radicals. A range of modest molecular weight random copolymers with varying DMA and TFME content was synthesised, including a terpolymer with oligo(ethylene glycol) methyl ether methacrylate. Coatings were produced by dissolving the polymers in DMF or ethyl acetate and drop-casting onto various substrates. A very interesting finer structure of the terpolymer coating was observed by SEM, showing a nano-ridged/wrinkled topography—which could be beneficial for antifouling purposes. Samples performed well in distilled water absorption tests (7 days, from 0.33 to 2.31%), and in a simple durability test by immersion for 7 days in 5% wt saline, 20% NaOH and 20% H<sub>2</sub>SO<sub>4</sub> solutions (all samples remained firmly attached on the substrate and showed minimal mass loss). Lastly, a qualitative antifouling test was performed by immersing a glass slide coated with the 50/50 DMA/TFME copolymer for 7 days in seawater, and comparing to a bare glass substrate by optical microscopy for attached fouling species; again the coated specimen outperformed the control.

## 5. Conclusions and Outlook

The research area of mussel-inspired synthetic polymers emerged in the mid-to-late 1980s and has since been prolific in terms of new structures reported [116] and possible applications (e.g., adhesives, biomedical, marine). In spite of the interest in producing polymers potentially suitable for marine antifouling coatings [101,136–143], issues remain with the scalability of the proposed chemistries and coating methods. In several of the approaches discussed, multi-step syntheses and significant purification efforts (column chromatography, dialysis) are needed to yield catechol-derivatised monomers and polymers. Moreover, the majority of marine antifouling testing reported here [101,136–143] has been on very small coupons (usually 10 mm × 10 mm) which were coated by a dip-coating approach (only one reference for a spray-based system [100]). Before any significant progress towards a commercially available and industrially applicable marine antifouling paint based on a mussel-inspired synthetic polymer, a focus on highly scalable chemistries would be necessary, along with an intense programme of at least demonstrator-scale (e.g., a painted panel of dimensions of several meters rather than centimeters) antifouling testing under static (simple immersion under controlled conditions) and dynamic (simulated flow conditions and field tests in seawater and freshwater) settings would be required. In this sense, a polymer modification approach (either main-chain or chain-end) of existing, otherwise suitable polymers with a catechol-bearing reagent may be a way forward—it only takes a few catechols to dramatically change the adhesion behavior. Non-covalent interactions and self-healing would also be useful attributes which could be gained by a modest presence of catechol moieties in the right structure. Lastly, one would need to

consider all the other parameters (presence of ions and ionic segments in the polymer, pH, interactions between hydrophobic segments, oxidants) which could affect the behavior of the catechol moiety. It is certain however that this research area will continue to propose structures and approaches at a high rate, and there will not be a lack of candidate materials.

**Funding:** The Institute of Technology Sligo and the Precision Engineering, Materials and Manufacturing (PEM) Research Centre are gratefully acknowledged for the provision of a postgraduate studentship to U.A. under the President's Bursary 2019 scheme (project code PPRES073).

**Acknowledgments:** Chemical structures and Schemes in this paper were produced with the ACD/ChemSketch Freeware (<https://www.acdlabs.com/resources/freeware/chemsketch/>).

**Conflicts of Interest:** The authors declare no conflict of interest.

## References

1. Callow, J.A.; Callow, M.E. Trends in the development of environmentally friendly fouling-resistant marine coatings. *Nat. Commun.* **2011**, *2*, 244–254. [[CrossRef](#)] [[PubMed](#)]
2. Marine Coating Market Estimated to Exceed \$15 Billion by End of 2024. Available online: [https://www.coatingsworld.com/contents/view\\_breaking-news/2017-03-01/marine-coating-market-estimated-to-exceed-15-billion-by-end-of-2024/#](https://www.coatingsworld.com/contents/view_breaking-news/2017-03-01/marine-coating-market-estimated-to-exceed-15-billion-by-end-of-2024/#) (accessed on 23 February 2020).
3. Schultz, M.P.; Bendick, J.A.; Holm, E.R.; Hertel, W.M. Economic impact of biofouling on a naval surface ship. *Biofouling* **2011**, *27*, 87–98. [[CrossRef](#)] [[PubMed](#)]
4. Bannister, J.; Sievers, M.; Bush, F.; Nina Bloecher, N. Biofouling in marine aquaculture: A review of recent research and developments. *Biofouling* **2019**, *35*, 631–648. [[CrossRef](#)]
5. Chambers, L.D.; Stokes, K.R.; Walsh, F.C.; Wood, R.J.K. Modern approaches to marine antifouling coatings. *Surf. Coat. Technol.* **2006**, *201*, 3642–3652. [[CrossRef](#)]
6. Anti-Fouling Systems. Available online: [http://www.imo.org/en/OurWork/Environment/Anti-foulingSystems/Pages/Default.aspx?\\_sm\\_au\\_=iVVVR7ZNM\]nDMQS57](http://www.imo.org/en/OurWork/Environment/Anti-foulingSystems/Pages/Default.aspx?_sm_au_=iVVVR7ZNM]nDMQS57) (accessed on 23 February 2020).
7. Kirschner, C.M.; Brennan, A.B. Bio-Inspired Antifouling Strategies. *Annu. Rev. Mater. Res.* **2012**, *42*, 211–229. [[CrossRef](#)]
8. The European Parliament and the Council of the European Union. Regulation (EU) No 528/2012 of the European Parliament and of the Council of 22 May 2012: Concerning the making available on the market and use of biocidal products. *Off. J. Eur. Union.* 27 June 2012.
9. World Coatings Council Submits Paper on Cybutryne to IMO Subcommittee. Available online: <https://www.paint.org/cybutryne/> (accessed on 21 March 2020).
10. Ciriminna, R.; Bright, F.V.; Pagliaro, M. Ecofriendly Antifouling Marine Coatings. *ACS Sustain. Chem. Eng.* **2015**, *3*, 559–565. [[CrossRef](#)]
11. Salta, M.; Wharton, J.A.; Stoodley, P.; Dennington, S.P.; Goodes, L.R.; Werwinski, S.; Mart, U.; Wood, R.J.K.; Stokes, K.R. Designing biomimetic antifouling surfaces. *Phil. Trans. R. Soc. A* **2010**, *368*, 4729–4754. [[CrossRef](#)]
12. Damodaran, V.B.; Murthy, N.S. Bio-inspired strategies for designing antifouling biomaterials. *Biomater. Res.* **2016**, *20*, 18–29. [[CrossRef](#)] [[PubMed](#)]
13. Cao, S.; Wang, J.-D.; Chen, H.-S.; Chen, D.-R. Progress of marine biofouling and antifouling technologies. *Chin. Sci. Bull.* **2011**, *56*, 598–612. [[CrossRef](#)]
14. Magin, C.M.; Cooper, S.P.; Brennan, A.B. Non-Toxic Antifouling Strategies. *Mater. Today* **2010**, *13*, 36–44. [[CrossRef](#)]
15. Waite, J.H.; Tanzer, M.L. Polyphenolic Substance of *Mytilus edulis*: Novel Adhesive Containing L-Dopa and Hydroxyproline. *Science* **1981**, *212*, 1038–1040. [[CrossRef](#)] [[PubMed](#)]
16. Meseguer Yebra, D.; Kiil, S.; Dam-Johansen, K. Antifouling technology—past, present and future steps towards efficient and environmentally friendly antifouling coatings. *Prog. Org. Coat.* **2004**, *50*, 75–104. [[CrossRef](#)]
17. Salta, M.; Wharton, J.A.; Blache, Y.; Stokes, K.R.; Briand, J.-F. Marine biofilms on artificial surfaces: Structure and dynamics. *Environ. Microbiol.* **2013**, *15*, 2879–2893. [[CrossRef](#)] [[PubMed](#)]

18. Dickinson, G.H.; Vega, I.E.; Wahl, K.J.; Orihuela, B.; Beyley, V.; Rodriguez, E.N.; Everett, R.K.; Bonaventura, J.; Daniel Rittschof, D. Barnacle cement: A polymerization model based on evolutionary concepts. *J. Exp. Biol.* **2009**, *212*, 3499–3510. [CrossRef] [PubMed]
19. Forooshani, P.K.; Lee, B.P. Recent Approaches in Designing Bioadhesive Materials Inspired by Mussel Adhesive Protein. *J. Polym. Sci. Part A Polym. Chem.* **2017**, *55*, 9–33. [CrossRef]
20. Lee, B.P.; Messersmith, P.B.; Israelachvili, J.N.; Waite, J.H. Mussel-Inspired Adhesives and Coatings. *Annu. Rev. Mater. Res.* **2011**, *41*, 99–132. [CrossRef]
21. Yu, M.; Hwang, J.; Deming, T.J. Role of L-3, 4-Dihydroxyphenylalanine in Mussel Adhesive Proteins. *J. Am. Chem. Soc.* **1999**, *121*, 5825–5826. [CrossRef]
22. Persson, F.; Svensson, R.; Nylund, G.M.; Fredriksson, N.J.; Pavia, H.; Hermansson, M. Ecological role of a seaweed secondary metabolite for a colonizing bacterial community. *Biofouling* **2011**, *27*, 579–588. [CrossRef]
23. Barrios, C.A.; Xu, Q.; Cutright, T.; Zhang Newby, B. Incorporating zosteric acid into silicone coatings to achieve its slow release while reducing fresh water bacterial attachment. *Colloids Surf. B Biointerfaces* **2005**, *41*, 83–93.col. [CrossRef]
24. Hao, E.; Fromont, J.; Jardine, D.; Karuso, P. Natural Products from Sponges of the Genus *Agelas*—on the Trail of a [2+2]-Photoaddition Enzyme. *Molecules* **2001**, *6*, 130–141. [CrossRef]
25. Stowe, S.D.; Richards, J.J.; Tucker, A.T.; Thompson, R.; Melander, M.; Cavanagh, J. Anti-Biofilm Compounds Derived from Marine Sponges. *Mar. Drugs* **2011**, *9*, 2010–2035. [CrossRef] [PubMed]
26. Zidar, N.; Montalvão, S.; Hodnik, Ž.; Nawrot, D.A.; Žula, A.; Ilaš, J.; Kikelj, D.; Tammela, P.; Peterlin Mašič, L. Antimicrobial Activity of the Marine Alkaloids, Clathrodin and Oroidin, and their Synthetic Analogues. *Mar. Drugs* **2014**, *12*, 940–963. [CrossRef] [PubMed]
27. Li, B.; Lu, F.; Wei, X.; Zhao, R. Fucoidan: Structure and Bioactivity. *Molecules* **2008**, *13*, 1671–1695. [CrossRef] [PubMed]
28. Ale, M.T.; Meyer, A.S. Fucoidans from brown seaweeds: An update on structures, extraction techniques and use of enzymes as tools for structural elucidation. *RSC Adv.* **2013**, *3*, 8131–8141. [CrossRef]
29. Jun, J.-Y.; Jung, M.; Jeong, I.-H.; Yamazaki, K.; Kawai, Y.; Kim, B.-M. Antimicrobial and Antibiofilm Activities of Sulfated Polysaccharides from Marine Algae against Dental Plaque Bacteria. *Mar. Drugs* **2018**, *16*, 301. [CrossRef] [PubMed]
30. Mohan, T.; Cas, A.; Bracič, M.; Plohl, O.; Vesel, A.; Rupnik, M.; Zemljic, L.F.; Rebol, J. Highly Protein Repellent and Antiadhesive Polysaccharide Biomaterial Coating for Urinary Catheter Applications. *ACS Biomater. Sci. Eng.* **2019**, *5*, 5825–5832. [CrossRef]
31. Wang, Y.; Xing, M.; Cao, Q.; Ji, A.; Liang, H.; Song, S. Biological Activities of Fucoidan and the Factors Mediating Its Therapeutic Effects: A Review of Recent Studies. *Mar. Drugs* **2019**, *17*, 183. [CrossRef]
32. Sharklet® Adhesively Backed Film. Available online: <https://www.sharklet.com/our-products/adhesively-backed-film/> (accessed on 10 April 2020).
33. Bohn, H.F.; Federle, W. Insect aquaplaning: *Nepenthes* pitcher plants capture prey with the peristome, a fully wettable water-lubricated anisotropic surface. *Proc. Natl. Acad. Sci. USA* **2004**, *101*, 14138–14143. [CrossRef]
34. Epstein, A.K.; Wong, T.-S.; Belisle, R.A.; Boggs, E.M.; Aizenberg, J. Liquid-infused structured surfaces with exceptional anti-biofouling performance. *Proc. Natl. Acad. Sci. USA* **2012**, *109*, 13182–13187. [CrossRef]
35. MacCallum, N.; Howell, C.; Kim, P.; Sun, D.; Friedlander, R.; Ranisau, J.; Ahanotu, O.; Lin, J.J.; Vena, A.; Hatton, B.; et al. Liquid-Infused Silicone as a Biofouling-Free Medical Material. *ACS Biomater. Sci. Eng.* **2015**, *1*, 43–51. [CrossRef]
36. Amini, S.; Kolle, S.; Petrone, L.; Ahanotu, O.; Sunny, S.; Sutanto, C.N.; Hoon, S.; Cohen, L.; Weaver, J.C.; Aizenberg, J.; et al. Preventing mussel adhesion using lubricant-infused materials. *Science* **2017**, *357*, 668–673. [CrossRef] [PubMed]
37. SLIPS® Foul Protect™ Bottom Paints from AST. Available online: <https://slipsfoulprotect.com/> (accessed on 12 April 2020).
38. Harrington, M.J.; Waite, J.H. Holdfast heroics: Comparing the molecular and mechanical properties of *Mytilus californianus* byssal threads. *J. Exp. Biol.* **2007**, *210*, 4307–4318. [CrossRef] [PubMed]
39. Waite, J.H. Mussel adhesion – essential footwork. *J. Exp. Biol.* **2017**, *220*, 517–530. [CrossRef]
40. Waite, J.H.; Qin, X.-X.; Coyne, K.J. The Peculiar Collagens of Mussel. Byssus. *Matrix Biol.* **1998**, *17*, 93–106. [CrossRef]

41. Waite, J.H. The formation of mussel byssus: Anatomy of a natural manufacturing process. In *Structure, Cellular Synthesis and Assembly of Biopolymers*, 1st ed.; Case, S.T., Ed.; Springer: Berlin/Heidelberg, Germany, 1992; Volume 19, pp. 27–54.
42. Waite, J.H. Evidence for a Repeating 3, 4-Dihydroxyphenylalanine and Hydroxyproline-containing Decapeptide in the Adhesive Protein of the Mussel, *Mytilus edulis* L. *J. Biol. Chem.* **1983**, *258*, 2911–2915. [[PubMed](#)]
43. Zhao, Y.; Waite, J.H. Linking Adhesive and Structural Proteins in the Attachment Plaque of *Mytilus californianus*. *J. Biol. Chem.* **2006**, *281*, 26150–26158. [[CrossRef](#)] [[PubMed](#)]
44. Yang, J.; Cohen Stuart, M.A.; Kamperman, M. Jack of all trades: Versatile catechol crosslinking mechanisms. *Chem. Soc. Rev.* **2014**, *43*, 8271–8298. [[CrossRef](#)]
45. Yu, J.; Wei, W.; Danner, E.; Ashley, R.K.; Israelachvili, J.N.; Waite, J.H. Mussel protein adhesion depends on interprotein thiol-mediated redox modulation. *Nat. Chem. Biol.* **2011**, *7*, 588–590. [[CrossRef](#)]
46. Miller, D.R.; Spahn, J.E.; Waite, J.H. The staying power of adhesion-associated antioxidant activity in *Mytilus californianus*. *J. R. Soc. Interface* **2015**, *12*, 614–621.
47. Jameson, G.N.L.; Zhang, J.; Jameson, R.F.; Linert, W. Kinetic evidence that cysteine reacts with dopaminoquinone via reversible adduct formation to yield 5-cysteinyldopamine: An important precursor of neuromelanin. *Org. Biomol. Chem.* **2004**, *2*, 777–782. [[CrossRef](#)]
48. Filippidi, E.; DeMartini, D.G.; Malo de Molina, P.; Danner, E.W.; Kim, J.; Helgeson, M.E.; Waite, J.H.; Valentine, M.T. The microscopic network structure of mussel (*Mytilus*) adhesive plaques. *J. R. Soc. Interface* **2015**, *12*, 827–837. [[CrossRef](#)] [[PubMed](#)]
49. Waite, J.H.; Vaccaro, E.; Sun, C.; Lucas, J.M. Elastomeric gradients: A hedge against stress concentration in marine holdfasts? *Phil. Trans. R. Soc. Lond. B* **2002**, *357*, 143–153. [[CrossRef](#)] [[PubMed](#)]
50. Harrington, M.J.; Gupta, H.S.; Fratzl, P.; Waite, J.H. Collagen insulated from tensile damage by domains that unfold reversibly: In situ X-ray investigation of mechanical yield and damage repair in the mussel byssus. *J. Struct. Biol.* **2009**, *167*, 47–54. [[CrossRef](#)]
51. McDowell, L.M.; Burzio, L.A.; Waite, H.J.; Schaefer, J. Rotational Echo Double Resonance Detection of Cross-links Formed in Mussel Byssus under High-Flow Stress. *J. Biol. Chem.* **1999**, *274*, 20293–20295. [[CrossRef](#)]
52. Holten-Andersen, N.; Fantner, G.; Hohlbauch, S.; Waite, J.H.; Zok, F.W. Protective coatings on extensible biofibres. *Nat. Mater.* **2007**, *6*, 669–672. [[CrossRef](#)] [[PubMed](#)]
53. Holten-Andersen, N.; Waite, J.H. Mussel-designed Protective Coatings for Compliant Substrates. *J. Dent. Res.* **2008**, *87*, 701–709. [[CrossRef](#)] [[PubMed](#)]
54. Holten-Andersen, N.; Mates, T.E.; Toprak, M.S.; Stucky, G.D.; Zok, F.W.; Waite, J.H. Metals and the Integrity of a Biological Coating: The Cuticle of Mussel Byssus. *Langmuir* **2009**, *25*, 3323–3326. [[CrossRef](#)] [[PubMed](#)]
55. Holten-Andersen, N.; Zhao, H.; Waite, J.H. Stiff Coatings on Compliant Biofibers: The Cuticle of *Mytilus californianus* Byssal Threads. *Biochemistry* **2009**, *48*, 2752–2759. [[CrossRef](#)] [[PubMed](#)]
56. Harrington, M.J.; Masic, A.; Holten-Andersen, N.; Waite, J.H.; Fratzl, P. Iron-Clad Fibers: A Metal-Based Biological Strategy for Hard Flexible Coatings. *Science* **2010**, *328*, 216–220. [[CrossRef](#)]
57. Liu, Y.; Meng, H.; Messersmith, P.B.; Lee, B.P.; Dalsin, J.L. Biomimetic Adhesives and Coatings Based on Mussel Adhesive Proteins. In *Biological Adhesives*, 2nd ed.; Smith, A.M., Ed.; Springer International Publishing: Cham, Switzerland, 2016; pp. 345–378.
58. Sever, M.J.; Wilker, J.J. Visible absorption spectra of metal–catecholate and metal–tironate complexes. *Dalton Trans.* **2004**, 1061–1072. [[CrossRef](#)]
59. Sever, M.J.; Wilker, J.J. Absorption spectroscopy and binding constants for first-row transition metal complexes of a DOPA-containing peptide. *Dalton Trans.* **2006**, 813–822. [[CrossRef](#)] [[PubMed](#)]
60. Monahan, J.; Wilker, J.J. Specificity of metal ion cross-linking in marine mussel adhesives. *Chem. Commun.* **2003**, 1672–1673. [[CrossRef](#)] [[PubMed](#)]
61. Dalsin, J.L.; Lin, L.; Tosatti, S.; Voros, J.; Textor, M.; Messersmith, P.B. Protein Resistance of Titanium Oxide Surfaces Modified by Biologically Inspired mPEG-DOPA. *Langmuir* **2005**, *21*, 640–646. [[CrossRef](#)]
62. Ribena, D.; Alekseev, A.; Van Asselen, O.; Mannie, G.J.; Hendrix, M.M.; van der Ven, L.G.; Sommerdijk, N.A.; de With, G. Significance of the Amide Functionality on DOPA-Based. Monolayers on Gold. *Langmuir* **2012**, *28*, 16900–16908. [[CrossRef](#)] [[PubMed](#)]

63. Lee, H.; Scherer, N.F.; Messersmith, P.B. Single-molecule mechanics of mussel adhesion. *Proc. Natl. Acad. Sci. USA* **2006**, *103*, 12999–13003. [[CrossRef](#)] [[PubMed](#)]
64. Holten-Andersen, N.; Harrington, M.J.; Birkedal, H.; Lee, B.P.; Messersmith, P.B.; Lee, K.Y.C.; Waite, J.H. pH-induced metal-ligand cross-links inspired by mussel yield self-healing polymer networks with near-covalent elastic moduli. *Proc. Natl. Acad. Sci. USA* **2011**, *108*, 2651–2655. [[CrossRef](#)]
65. Lee, H.; Dellatore, S.M.; Miller, W.M.; Messersmith, P.B. Mussel-Inspired Surface Chemistry. For Multifunctional Coatings. *Science* **2007**, *318*, 426–430. [[CrossRef](#)]
66. He, L.; Fullenkamp, D.E.; Rivera, J.G.; Messersmith, P.B. pH responsive self-healing hydrogels formed by boronate–catechol complexation. *Chem. Commun.* **2011**, *47*, 7497–7499. [[CrossRef](#)]
67. Narkar, A.R.; Barker, B.; Clisch, M.; Jiang, J.; Lee, B.P. pH Responsive and Oxidation Resistant Wet Adhesive based on Reversible Catechol–Boronate Complexation. *Chem. Mater.* **2016**, *28*, 5432–5439. [[CrossRef](#)]
68. Springsteen, G.; Wang, B. A detailed examination of boronic acid-diol complexation. *Tetrahedron* **2000**, *58*, 5291–5300. [[CrossRef](#)]
69. Yan, J.; Springsteen, G.; Deeter, S.; Wang, B. The relationship among pKa, pH, and binding constants in the. Interactions between boronic acids and diols—It is not as simple as it appears. *Tetrahedron* **2004**, *60*, 11205–11209. [[CrossRef](#)]
70. Hofman, A.H.; van Hees, I.A.; Yang, J.; Kamperman, M. Bioinspired Underwater Adhesives by Using the Supramolecular Toolbox. *Adv. Mater.* **2018**, *30*, 1704640–1704678. [[CrossRef](#)] [[PubMed](#)]
71. Wei, W.; Yu, J.; Gebbie, M.A.; Tan, Y.; Nadine, R.; Martinez Rodriguez, N.R.; Israelachvili, J.N.; Waite, J.H. Bridging Adhesion of Mussel-Inspired Peptides: Role of Charge, Chain Length, and Surface Type. *Langmuir* **2015**, *31*, 1105–1112. [[CrossRef](#)] [[PubMed](#)]
72. Yu, J.; Kan, Y.; Rappa, M.; Danner, E.; Wei, W.; Das, S.; Miller, D.S.; Chen, Y.; Waite, J.H.; Israelachvili, J.N. Adaptive hydrophobic and hydrophilic interactions of mussel foot proteins with organic thin films. *Proc. Natl. Acad. Sci. USA* **2013**, *110*, 15680–15685. [[CrossRef](#)]
73. Lu, Q.; Danner, E.; Waite, J.H.; Israelachvili, J.N.; Zeng, H.; Hwang, D.S. Adhesion of mussel foot proteins to different substrate surfaces. *J. R. Soc. Interface* **2013**, *10*, 20120759–20120770. [[CrossRef](#)]
74. Ahn, B.K.; Lee, D.W.; Israelachvili, J.N.; Waite, J.H. Surface-initiated self-healing of polymers in aqueous media. *Nat. Mater.* **2014**, *13*, 867–872. [[CrossRef](#)]
75. Shannon, A.; Manolakis, I. A Facile Route to Bio-Inspired Supramolecular Oligo (Ethylene Glycol) Catecholates. *Macromol. Chem. Phys.* **2019**, *220*, 1800412–1800418. [[CrossRef](#)]
76. Brown, C.J. The Crystal Structure of Catechol. *Acta Cryst.* **1966**, *21*, 170–174. [[CrossRef](#)]
77. Yamamoto, H. Synthesis and Adhesive Studies of Marine Polypeptides. *J. Chem. Soc. Perkin Trans I* **1987**. [[CrossRef](#)]
78. Harwood, H.J.; Cassidy, H.G. Electron Exchange Polymers. IX. Synthesis of Polymers of 2, 5-Dihydroxy phenylalanine and of 3, 4-Dihydroxyphenylalanine (DOPA). *J. Am. Chem. Soc.* **1957**, *79*, 4360–4365. [[CrossRef](#)]
79. Yamamoto, H.; Hayakawa, T. Sense of Helix of Poly-O, O'-dicarbobenzoxy-L-DOPA in Solution. *Macromolecules* **1976**, *9*, 532–534. [[CrossRef](#)]
80. Yamamoto, H.; Hayakawa, T. Synthesis and conformational study of poly (l-β-3, 4-dihydroxyphenyl-α-alanine). *Polymer* **1977**, *18*, 979–983. [[CrossRef](#)]
81. Fuller, W.D.; Verlander, M.S.; Goodman, M. DOPA-Containing Polypeptides. I. Improved Synthesis of High-Molecular-Weight Poly (L-DOPA) and Water-Soluble Copolypeptides. *Biopolymers* **1978**, *17*, 2939–2943. [[CrossRef](#)]
82. Yu, M.; Deming, T.J. Synthetic Polypeptide Mimics of Marine Adhesives. *Macromolecules* **1998**, *31*, 4739–4745. [[CrossRef](#)] [[PubMed](#)]
83. Statz, A.R.; Meagher, R.J.; Barron, A.E.; Messersmith, P.B. New Peptidomimetic Polymers for Antifouling Surfaces. *J. Am. Chem. Soc.* **2005**, *127*, 7972–7973. [[CrossRef](#)]
84. Statz, A.R.; Barron, A.E.; Messersmith, P.B. Protein, cell and bacterial fouling resistance of polypeptoid modified surfaces: Effect of side-chain chemistry. *Soft Matter* **2008**, *4*, 131–139. [[CrossRef](#)]
85. Statz, A.R.; Park, J.P.; Chongsiriwatana, N.P.; Barron, A.E.; Messersmith, P.B. Surface-immobilized antimicrobial peptoids. *Biofouling* **2008**, *24*, 439–448. [[CrossRef](#)]
86. Lee, J.H.; Lee, H.B.; Andrade, J.D. Blood Compatibility of Polyethylene Oxide Surfaces. *Prog. Polym. Sci.* **1995**, *20*, 1043–1079. [[CrossRef](#)]

87. Schlenoff, J.B. Zwitteration: Coating Surfaces with Zwitterionic Functionality to Reduce Nonspecific Adsorption. *Langmuir* **2014**, *30*, 9625–9636. [[CrossRef](#)]
88. Lin, W.; Klein, J. Control of surface forces through hydrated boundary layers. *Curr. Opin. Coll. Interf. Sci.* **2019**, *44*, 94–106. [[CrossRef](#)]
89. Huang, K.; Lee, B.P.; Ingram, D.I.; Messersmith, P.B. Synthesis and Characterization of Self-Assembling Block Copolymers Containing Bioadhesive End Groups. *Biomacromolecules* **2002**, *3*, 397–406. [[CrossRef](#)]
90. Lee, B.P.; Dalsin, J.L.; Messersmith, P.B. Synthesis and Gelation of DOPA-Modified Poly (ethylene glycol) Hydrogels. *Biomacromolecules* **2002**, *3*, 1038–1047. [[CrossRef](#)]
91. Brubaker, C.E.; Kissler, H.; Wang, L.-J.; Kaufman, D.B.; Messersmith, P.B. Biological performance of mussel-inspired adhesive in extrahepatic islet transplantation. *Biomaterials* **2010**, *31*, 420–427. [[CrossRef](#)]
92. Wei Zhang, W.; Wang, R.; Sun, Z.M.; Zhu, X.; Zhao, Q.; Zhang, T.; Cholewinski, A.; Yang, F.K.; Zhao, B.; Pinnaratip, R.; et al. Catechol-functionalized hydrogels: Biomimetic design, adhesion mechanism, and biomedical applications. *Chem. Soc. Rev.* **2020**, *49*, 433–464. [[CrossRef](#)]
93. Lee, H.; Lee, K.D.; Pyo, K.B.; Park, S.Y.; Lee, H. Catechol-Grafted Poly (ethylene glycol) for PEGylation on Versatile Substrates. *Langmuir* **2010**, *26*, 3790–3793. [[CrossRef](#)]
94. Khalila, F.; Franzmann, E.; Julian Ramcke, J.; Dakischew, O.; Lips, K.S.; Reinhardt, A.; Heisig, P.; Maison, W. Biomimetic PEG-catecholates for stable antifouling coatings on metal surfaces: Applications on TiO<sub>2</sub> and stainless steel. *Colloids Surf. B Biointerfaces* **2014**, *117*, 185–192. [[CrossRef](#)] [[PubMed](#)]
95. Manolakis, I.; Noordover, B.A.J.; Vendamme, R.; Eevers, W. Novel-DOPA-Derived Poly (ester amide) s: Monomers, Polymers, and the First L-DOPA-Functionalized Biobased Adhesive Tape. *Macromol. Rapid Commun.* **2014**, *35*, 71–76. [[CrossRef](#)]
96. Sunder, A.; Hanselmann, R.; Frey, H.; Müllhaupt, R. Controlled Synthesis of Hyperbranched Polyglycerols by Ring-Opening Multibranching Polymerization. *Macromolecules* **1999**, *32*, 4240–4246. [[CrossRef](#)]
97. Frey, H.; Haag, R. Dendritic polyglycerol: A new versatile biocompatible material. *Rev. Mol. Biotechnol.* **2002**, *90*, 257–267. [[CrossRef](#)]
98. Wei, Q.; Krysiak, S.; Achazi, K.; Becherer, T.; Noeske, P.-L.M.; Paulus, F.; Liebe, H.; Grunwald, I.; Dervedde, J.; Hartwig, A.; et al. Multivalent anchored and crosslinked hyperbranched polyglycerol monolayers as antifouling coating for titanium oxide surfaces. *Colloids Surf. B Biointerfaces* **2014**, *122*, 684–692. [[CrossRef](#)]
99. Wei, Q.; Achazi, K.; Liebe, H.; Schulz, A.; Noeske, P.-L.M.; Grunwald, I.; Haag, R. Mussel-Inspired Dendritic Polymers as Universal Multifunctional Coatings. *Angew. Chem. Int. Ed.* **2014**, *53*, 11650–11655. [[CrossRef](#)]
100. Schlaich, C.; Li, M.; Cheng, C.; Donskyi, I.S.; Yu, L.; Song, G.; Osorio, E.; Wei, Q.; Haag, R. Mussel-Inspired Polymer-Based Universal Spray Coating for Surface Modification: Fast Fabrication of Antibacterial and Superhydrophobic Surface Coatings. *Adv. Mater. Interfaces* **2018**, *5*, 1701254–1701262. [[CrossRef](#)]
101. Pranantyo, D.; Xu, L.Q.; Neoh, K.G.; Kang, E.-T.; Lay-Ming Teo, S. Antifouling Coatings via Tethering of Hyperbranched Polyglycerols on Biomimetic Anchors. *Ind. Eng. Chem. Res.* **2016**, *55*, 1890–1901. [[CrossRef](#)]
102. Westwood, G.; Horton, T.N.; Wilker, J.J. Simplified Polymer Mimics of Cross-Linking Adhesive Proteins. *Macromolecules* **2007**, *40*, 3960–3964. [[CrossRef](#)]
103. Matos-Pérez, C.R.; White, J.D.; Wilker, J.J. Polymer Composition and Substrate Influences on the Adhesive Bonding of a Biomimetic, Cross-Linking Polymer. *J. Am. Chem. Soc.* **2012**, *134*, 9498–9505.
104. White, J.D.; Wilker, J.J. Underwater Bonding with Charged Polymer Mimics of Marine. Mussel Adhesive Proteins. *Macromolecules* **2011**, *44*, 5085–5088. [[CrossRef](#)]
105. Matos-Pérez, C.R.; Wilker, J.J. Ambivalent Adhesives: Combining Biomimetic Cross-Linking with. Antiadhesive Oligo (ethylene glycol). *Macromolecules* **2012**, *45*, 6634–6639. [[CrossRef](#)]
106. Chung, H.; Glass, P.; Pothen, J.M.; Sitti, M.; Washburn, N.R. Enhanced Adhesion of Dopamine Methacrylamide Elastomers via Viscoelasticity Tuning. *Biomacromolecules* **2011**, *12*, 342–347. [[CrossRef](#)]
107. Zhang, H.; Zhao, T.; Newland, B.; Liu, W.; Wang, W.; Wang, W. Catechol functionalized hyperbranched polymers as biomedical materials. *Prog. Pol. Sci.* **2018**, *78*, 47–55. [[CrossRef](#)]
108. Zhang, H.; Zhao, T.; Newland, B.; Duffy, P.; Ni Annaidh, A.; O’Cearbhaill, E.D.; Wang, W. On-demand and negative-thermo-swelling tissue adhesive based on highly branched ambivalent PEG–catechol copolymers. *J. Mater. Chem. B* **2015**, *3*, 6420–6428. [[CrossRef](#)]
109. Breydo, L.; Newland, B.; Zhang, H.; Rosser, A.; Werner, C.; Uversky, V.N.; Wang, W. A Hyperbranched Dopamine-Containing PEG-based Polymer for the Inhibition of  $\alpha$ -Synuclein Fibrillation. *Biochem. Biophys. Res. Commun.* **2016**, *469*, 830–835. [[CrossRef](#)]

110. Wu, J.; Zhang, L.; Wang, Y.; Long, Y.; Gao, H.; Zhang, X.; Zhao, N.; Cai, Y.; Xu, J. Mussel-Inspired Chemistry for Robust and Surface-Modifiable Multilayer Films. *Langmuir* **2011**, *27*, 13684–13691. [[CrossRef](#)]
111. Solovskij, M.V.; Denisov, V.M.; Panarin, E.E.; Petukhova, N.A.; Purkina, A.V. Synthesis of water-soluble biologically active phenol (or catechol) containing copolymers of N-vinyl-2-pyrrolidone. *Macromol. Chem. Phys.* **1996**, *197*, 2035–2046. [[CrossRef](#)]
112. Laulicht, B.; Mancini, A.; Geman, N.; Cho, D.; Estrellas, K.; Furtado, S.; Hopson, R.; Tripathi, A.; Mathiowitz, E. Bioinspired Bioadhesive Polymers: Dopa-Modified Poly(acrylic acid) Derivatives. *Macromol. Biosci.* **2012**, *12*, 1555–1565. [[CrossRef](#)]
113. Zhou, J.; Defante, A.P.; Lin, F.; Xu, Y.; Yu, J.; Gao, Y.; Childers, E.; Dhinojwala, A.; Becker, M.L. Adhesion Properties of Catechol-Based Biodegradable Amino Acid-Based Poly(ester urea) Copolymers Inspired from Mussel Proteins. *Biomacromolecules* **2015**, *16*, 266–274. [[CrossRef](#)]
114. Xu, Y.; Liu, Q.; Narayanan, A.; Jain, D.; Dhinojwala, A.; Joy, A. Mussel-Inspired Polyesters with Aliphatic Pendant Groups Demonstrate the Importance of Hydrophobicity in Underwater Adhesion. *Adv. Mater. Interfaces* **2017**, *4*, 1700506–1700512. [[CrossRef](#)]
115. Mehdizadeh, M.; Weng, H.; Gyawali, D.; Tang, L.; Yang, J. Injectable citrate-based mussel-inspired tissue bioadhesives with high wet strength for sutureless wound closure. *Biomaterials* **2012**, *33*, 7972–7983. [[CrossRef](#)]
116. Patil, N.; Jérôme, C.; Detrembleur, C. Recent advances in the synthesis of catechol-derived (bio) polymers for applications in energy storage and environment. *Prog. Pol. Sci.* **2018**, *82*, 34–91. [[CrossRef](#)]
117. Wang, X.; Jiang, Z.; Shi, J.; Zhang, C.; Zhang, W.; Wu, H. Dopamine-Modified Alginate Beads Reinforced by Cross-Linking via Titanium Coordination or Self-Polymerization and Its Application in Enzyme Immobilization. *Ind. Eng. Chem. Res.* **2013**, *52*, 14828–14836. [[CrossRef](#)]
118. Alegre-Requena, J.V.; Häring, M.; Herrera, R.P.; Diaz Diaz, D. Regulatory parameters of self-healing alginate hydrogel networks prepared via mussel-inspired dynamic chemistry. *New J. Chem.* **2016**, *40*, 8493–8501. [[CrossRef](#)]
119. Hyun Ryu, J.; Lee, Y.; Kong, W.H.; Kim, T.G.; Tae Gwan Park, T.G.; Lee, H. Catechol-Functionalized Chitosan/Pluronic Hydrogels for Tissue Adhesives and Hemostatic Materials. *Biomacromolecules* **2011**, *12*, 2653–2659.
120. Kim, K.; Hyun Ryu, J.; Lee, D.Y.; Lee, H. Bio-inspired catechol conjugation converts water-insoluble chitosan into a highly water-soluble, adhesive chitosan derivative for hydrogels and LbL assembly. *Biomater. Sci.* **2013**, *1*, 783–790. [[CrossRef](#)]
121. Kim, K.; Kim, K.; Hyun Ryu, J.; Lee, H. Chitosan-catechol: A polymer with long-lasting mucoadhesive properties. *Biomaterials* **2015**, *52*, 161–170. [[CrossRef](#)]
122. Hyun Ryu, J.; Hong, S.; Lee, H. Bio-inspired adhesive catechol-conjugated chitosan for biomedical applications: A mini review. *Acta Biomater.* **2015**, *27*, 101–115.
123. Ways, T.M.W.; Lau, W.M.; Khutoryanskiy, V.V. Chitosan and Its Derivatives for Application in Mucoadhesive Drug Delivery Systems. *Polymers* **2018**, *10*, 267. [[CrossRef](#)]
124. Lee, Y.; Chung, H.J.; Yeo, S.; Ahn, C.-H.; Lee, H.; Messersmith, P.B.; Park, T.G. Thermo-sensitive, injectable, and tissue adhesive sol–gel transition hyaluronic acid/pluronic composite hydrogels prepared from bio-inspired catechol-thiol reaction. *Soft Matter* **2010**, *6*, 977–983. [[CrossRef](#)]
125. Jeong, Y.; Thuy, L.T.; Ki, S.H.; Ko, S.; Kim, S.; Cho, K.W.; Choi, J.S.; Kang, S.M. Multipurpose Antifouling Coating of Solid Surfaces with the Marine-Derived Polymer Fucoidan. *Macromol. Biosci.* **2018**, *18*, 1800137–1800144. [[CrossRef](#)]
126. Lee, M.; Kim, Y.; Hyun Ryu, J.; Kim, K.; Han, Y.-M.; Lee, H. Long-term, feeder-free maintenance of human embryonic stem cells by mussel-inspired adhesive heparin and collagen type I. *Acta Biomater.* **2016**, *32*, 138–148. [[CrossRef](#)]
127. Kim, S.; Ko, S.; Kang, S.M. Adhesive Heparin Coating for Marine Antifouling Applications. *Macromol. Res.* **2016**, *24*, 645–649. [[CrossRef](#)]
128. Hyun Ryu, J.; Messersmith, P.B.; Lee, H. Polydopamine Surface Chemistry: A Decade of Discovery. *ACS Appl. Mater. Interfaces* **2018**, *10*, 7523–7540.
129. Lee, H.A.; Ma, Y.; Zhou, F.; Hong, S.; Lee, H. Material-Independent Surface Chemistry beyond Polydopamine Coating. *Acc. Chem. Res.* **2019**, *52*, 704–713. [[CrossRef](#)]
130. Liebscher, J. Chemistry of Polydopamine—Scope, Variation, and Limitation. *Eur. J. Org. Chem.* **2019**, *31*, 4976–4994. [[CrossRef](#)]

131. Wang, Z.; Yang, H.-C.; He, F.; Peng, S.; Li, Y.; Shao, L.; Darling, S.B. Mussel-Inspired Surface Engineering for Water-Remediation Materials. *Matter* **2019**, *1*, 115–155. [[CrossRef](#)]
132. Xi, Z.-Y.; Xu, Y.-Y.; Zhu, L.-P.; Wang, Y.; Zhu, B.-K. A facile method of surface modification for hydrophobic polymer membranes based on the adhesive behavior of poly (DOPA) and poly(dopamine). *J. Membr. Sci.* **2009**, *327*, 244–253. [[CrossRef](#)]
133. Lu, Z.; Douek, A.M.; Rozario, A.M.; Tabor, R.F.; Kaslin, J.; Follink, B.; Teo, B.M. Bioinspired polynorepinephrine nanoparticles as an efficient vehicle for enhanced drug delivery. *J. Mater. Chem. B* **2020**, *8*, 961–968. [[CrossRef](#)] [[PubMed](#)]
134. Malollari, K.G.; Delparastan, P.; Sobek, C.; Vachhani, S.J.; Fink, T.D.; Zha, R.H.; Messersmith, P.B. Mechanical Enhancement of Bioinspired Polydopamine Nanocoatings. *ACS Appl. Mater. Interfaces* **2019**, *11*, 43599–43607. [[CrossRef](#)]
135. Saiz-Poseu, J.; Sedó, J.; García, B.; Benaiges, C.; Parella, T.; Alibés, R.; Hernando, J.; Busqué, F.; Ruiz-Molina, D. Versatile Nanostructured Materials via Direct Reaction of Functionalized Catechols. *Adv. Mater.* **2013**, *25*, 2066–2070. [[CrossRef](#)]
136. Yeon, D.K.; Ko, S.; Jeong, S.; Hong, S.-P.; Kang, S.M.; Cho, W.K. Oxidation-Mediated, Zwitterionic Polydopamine Coatings for Marine Antifouling Applications. *Langmuir* **2019**, *35*, 1227–1234. [[CrossRef](#)]
137. Hong, J.; Jwa, D.G.; Ha, H.; Kwak, J.; Kim, M.; Kang, S.M. 4-(3-Aminopropyl)-benzene-1,2-diol: An Improved Material-Independent Surface-Coating Reagent Compared to Dopamine. *Langmuir* **2019**, *35*, 6898–6904. [[CrossRef](#)]
138. He, M.; Gao, K.; Zhou, L.; Jiao, Z.; Wu, M.; Cao, J.; You, X.; Cai, Z.; Su, Y.; Jiang, Z. Zwitterionic materials for antifouling membrane surface construction. *Acta Biomater.* **2016**, *40*, 142–152. [[CrossRef](#)]
139. Kim, S.; Gim, T.; Jeong, Y.; Ryu, J.H.; Kang, S.M. Facile Construction of Robust Multilayered PEG Films on Polydopamine-Coated Solid Substrates for Marine Antifouling Applications. *ACS Appl. Mater. Interfaces* **2018**, *10*, 7626–7631. [[CrossRef](#)] [[PubMed](#)]
140. Kang, T.; Banquy, X.; Heo, J.; Lim, C.; Lynd, N.A.; Lundberg, P.; Oh, D.X.; Lee, H.-K.; Hong, Y.-K.; Hwang, D.S.; et al. Mussel-Inspired Anchoring of Polymer Loops That Provide Superior Surface Lubrication and Antifouling Properties. *ACS Nano* **2016**, *10*, 930–937. [[CrossRef](#)] [[PubMed](#)]
141. Cao, P.; Dub, C.; He, X.; Zhang, C.; Yuan, C. Modification of a derived antimicrobial peptide on steel surface for marine bacterial resistance. *Appl. Surf. Sci.* **2020**, *510*, 145512–145520. [[CrossRef](#)]
142. Wang, J.; He, C. Photopolymerized biomimetic self-adhesive Polydimethylsiloxane-based amphiphilic cross-linked coating for anti-biofouling. *Appl. Surf. Sci.* **2019**, *463*, 1097–1106. [[CrossRef](#)]
143. Sun, Q.; Lia, H.; Xian, C.; Yang, Y.; Song, Y.; Cong, P. Mimetic marine antifouling films based on fluorine-containing polymethacrylates. *Appl. Surf. Sci.* **2015**, *344*, 17–26. [[CrossRef](#)]

